MSc Thesis Biomedical Engineering

Sensitivity Analysis of a Parametric Optimization Model Used to Identify Neural and Non-Neural Contributors to Joint Stiffness

Ricardo Melvin Bouman
January 20, 2025

Master of Science - Biomedical Engineering

Sensitivity Analysis of a Parametric Optimization Model Used to Identify Neural and Non-Neural Contributors to Joint Stiffness

Ricardo Melvin Bouman

A thesis submitted to the Delft University of Technology in partial fulfillment of the requirements for the degree Master of Science in Biomedical Engineering

January 20, 2025

Supervisors:
Dr. Ir. W. Mugge
Dr. Ir. J.H. de Groot
Prof.dr.ir. A.C. Schouten

Preface

Through this study, I aimed to contribute to the advancement of a parametric optimization model with the hope that, in the future, individuals with spasticity will benefit from improved treatments and, ultimately, a higher quality of life. I have always been an active person and exercising weekly has greatly benefited my mental health. I have long felt compassion and respect for those who, due to physical limitations, are unable to move as freely as I can and still stay positive.

The scope of this work involved setting up an experimental sensitivity analysis, using the resulting data to test and better understand the behavior of the computer model. My research question centers on understanding how changes in the intrinsic properties of mass, misalignment, and stiffness impact the experimental outcomes of a robotic manipulator, and how effectively the parametric optimization model captures these effects.

Throughout this journey, I have been fortunate to have the support and guidance of several individuals. I would like to thank my supervisors — Dr.ir. W. Mugge, Dr.ir J.H. de Groot, and Prof.dr.ir. A.C. Schouten — and PhD staff member M.L. van de Ruit for their invaluable insights and encouragement. Their support has been essential in helping me navigate this research and in fostering an open dialogue around mental health in the academic community.

This work is particularly relevant because it aims to make spasticity more quantifiable. By identifying the neural and non-neural contributors to stiffness caused by spasticity, we can pave the way for more tailored and effective treatments, which could lead to better mobility for people living with this condition. Currently, there is a gap in knowledge regarding a computer model designed in collaboration between the TU Delft and Leiden University Medical Center. Some parameters in this model act erratically, and with the large number of parameters involved, it becomes difficult to fully understand the model's behavior. This study investigates whether the model can effectively capture changes in mass, stiffness, and alignment, similar to the results observed in real-life experiments.

I encountered several challenges while conducting this research, particularly with the robotic manipulator, of which two had a significant impact on the outcome. For the inertia measurement test involving a multi-sine perturbation, I had to limit the amplitude to just 10% of a participant's range of motion to avoid drifting. Although the underlying model of the manipulator recognized the offset, it failed to correct it. Moreover, the robot broke down after testing only two participants, preventing me from testing more subjects. I had originally planned to also test a newly designed foothold, but this was not possible as the robot broke down before the foothold was fully realized. Despite these setbacks, I persevered, driven by the importance of this work and the hope that my contributions will facilitate the future development of the computer model.

Finally, I would like to dedicate this work to my family, whose unwavering support has been instrumental throughout this journey. Their encouragement and belief in me have been a constant source of strength.

Contents

Abbreviations

$A1$	Alignment 1
$A2$	Alignment 2
CoM	Center of mass
CS	Coördinate system
DF	Dorsiflexion
DoF	Degree of freedom
EMG	Electromyograph
GL	M. gastrocnemius lateralis
GM	M. gastrocnemius medialis
$K1$	Added spring 1
$K2$	Added spring 2
$M1$	Added mass 1
$M2$	Added mass 2
MAS	Modified Ashworth scale
PF	Plantar flexion
$RMSE$	Root mean square error
RoM	Range of motion
SOL	M. soleus
TA	M. tibialis anterior
TS	M. triceps surea
VAF	Variance accounted for

Master thesis **2025**

Sensitivity Analysis Of A Parametric Optimization Model Used For The Identification of Neural and Non-Neural Contributors to Joint Stiffness

Ricardo Melvin Bouman

Department of BioMechanical Engineering, Faculty of Mechanical Engineering
Delft University of Technology, 2628 CD Delft, The Netherlands

Abstract. The influence of intrinsic properties (mass, stiffness, and alignment) on ankle joint dynamics, along with the sensitivity of a parametric optimization model to changes in these properties, was investigated. Experiments were performed on two young adults using a robotic manipulator to apply controlled perturbations comprising multiple ramp-and-holds while recording position, torque, and electromyography (EMG) data. Position, torque, and EMG data were subsequently used as input for the computational model, producing a modeled torque. The model, designed to parametrize neural and non-neural contributors to joint stiffness associated with spasticity, employs a 23-parameter Hill-type neuromuscular framework to estimate muscle properties by minimizing the difference between modeled and measured torque. Experimental results revealed that mass and stiffness significantly influenced the required torque, particularly during the hold phases, while alignment had minimal effects. Model sensitivity analysis showed similar trends, with stiffness having the greatest impact on torque, followed by mass. Changes in alignment were minimal, highlighting its redundancy. Discrepancies were observed between model predictions and experimental data in capturing the effects of mass and stiffness changes. The model predicted equivalent mass effects regardless of angle, whereas experimental data exhibited angle dependency. Furthermore, modifying stiffness did not affect the dynamic phases of the modeled torque but did influence the dynamic phases of the measured torque. These findings highlight the complex interplay between biomechanical factors and torque generation. Future work should refine the model to capture physical nuances better, improve experimental setups to control joint angles and optimize model parameters in a staged approach. Such efforts will advance the development of the model and deepen the understanding of spasticity, paving the way for more accurate and personalized treatment strategies.

KEY WORDS: Spasticity; neural; non-neural; sensitivity analysis; Parametric; Optimization; Model

1 Introduction

The ability of humans to move around has significantly improved with technological advancements. However, this progress has not always benefited individuals suffering from spasticity. While the healthy population seamlessly adapts to increased mobility in areas such as transportation and urban environments, individuals with spasticity face significant challenges in adapting. This limited adaptability negatively affects various aspects of their daily functioning, including physical tasks, social participation, and independence [1]. Consequently, individuals with spasticity often experience a diminished quality of life, reduced overall well-being, and fewer opportunities for education and employment [2].

The disparity between the healthy and affected populations frequently leads to stigmatization and accessibility challenges, as societal infrastructure is often not designed to meet their needs [3–6]. Moreover, access to high-quality healthcare is essential for treating individuals with spasticity. This includes personalized treatment plans tailored to their specific neurological and functional impairments [7–9]. In other words, the impact of spasticity extends beyond medical implications, affecting nearly every aspect of the life of a person.

Spasticity is a motor disorder arising from neurological conditions that affect the upper motor neurons or brain. Lance provides the most widely recognized definition, describing spasticity as "a motor disorder characterized by a velocity-dependent increase in tonic stretch reflexes with exaggerated tendon jerks, resulting from hyper-excitability of the stretch reflex" [10]. The definition of Lance aligns with observations of velocity-dependent resistance to movement and changes in short- and medium-latency responses in electromyography (EMG) signals [11–23]. However, many studies have not reported acceleration profiles or have shown concurrent increases in both acceleration and velocity. This leaves the ambiguity of whether spasticity is primarily dependent on velocity or acceleration.

Early research in 1983 suggested a potential link between acceleration and the stretch reflex [24]. Recent studies have revisited the idea of an acceleration dependency, challenging the definition of Lance [25–29]. However, conflicting findings persist, leaving uncertainty as to whether spasticity is primarily velocity-, acceleration-, or even force-dependent [14, 28, 30].

Progress has been made in understanding the mechanisms underlying spasticity since its characteristic stiffness was first described in patients with spinal cord injuries [31]. Individuals with spasticity experience hypertonia, caused by a combination of hyperreflexia and increased tissue stiffness, resulting in a reduced range of motion (RoM) [11, 12, 32–37]. Hyperreflexia occurs due to the hyper-excitability of the muscle's excitatory systems, creating an imbalance between inhibitory and excitatory mechanisms [38]. Advances in this field have clarified the roles of neural and biomechanical factors, but quantifying them is still a researched topic.

Various scales have been developed to quantify and categorize the intensity of spasticity. The Modified Ashworth Scale (MAS) categorizes muscle tone across the passive range of motion of a joint. Despite its widespread use, the MAS provides only qualitative information and lacks objectivity and sensitivity. Furthermore, the MAS cannot differentiate between neural and non-neural components of spasticity and fails to account for its potential velocity-dependence [36, 39–41]. The Tardieu Scale offers a more objective alternative by considering the velocity-dependency. However, its validity and reliability are still questioned, highlighting the need for further improvements in spasticity assessment tools [42–45].

Manual assessments like the MAS and Tardieu Scale are prone to variability and reduce reliability, due to subjective interpretation and inconsistent application. In contrast, motorized assessments provide objective measurements by enabling precise control of the end-effector, minimizing undesired movements during testing. Additionally, motorized systems can quantify the neural and non-neural components of spasticity by incorporating computer models [11, 46–51].

Distinguishing whether spastic complications arise from neural or non-neural components is crucial for selecting the appropriate treatment, as interventions target either neural or non-neural mechanisms [52, 53]. Objectively quantifying the neural or non-neural impairments provides essential information to personalize treatment, improving the overall effectiveness and outcome [54].

Approaches to objectively quantify the neural and non-neural components of spasticity rely on measurements of biomechanical and neurophysiological properties [11, 46–51, 55]. These studies typically involve passively stretching a joint through its RoM using a motorized manipulator, while recording torque and EMG. By applying parametric neuromuscular optimization models to the measured data, the neural and non-neural components were estimated [56].

One such parametric optimization model is being developed collaboratively by TU Delft and Leiden University Medical Center (LUMC) [11, 46–51]. While the model captures differences between participants, certain parameters related to inertia, such as mass and misalignment, are optimized erratically. The mass and misalignment often converge to the extreme bounds of the optimization range, failing to exhibit stable or meaningful trends. The research presented in this paper investigated the influence of mass and alignment, along with one of the principal determinants, stiffness. A sensitivity analysis was conducted both exper-

imentally and within the computational model to address the research question:

How effectively does the parametric optimization model, used to identify neural and non-neural contributors to joint stiffness, capture the effects of changes in intrinsic properties such as mass, misalignment, and stiffness?

1.1 Approach

The behavior of a computational model designed to quantify spasticity was investigated and mapped through sensitivity analysis and experimental validation. Specifically, the computer model created by the collaboration between the TU Delft and the LUMC [11, 46–51]. Experimentally, joint dynamics of the ankle were examined using a robotic manipulator that applied one-degree-of-freedom ramp-and-hold perturbations in the sagittal plane.

The sensitivity analysis focused on three key characteristics: mass, stiffness, and alignment. Experimentally, a participant was positioned in the robotic manipulator in a standardized configuration. The protocol began with a baseline trial to establish reference data. Subsequently, six test conditions were introduced, two with additional mass, two with added stiffness, and two with altered alignment. The mass was modified by attaching a weight to the foothold of the manipulator. The stiffness was adjusted by securing a spring to the heel end of the foothold. The alignment was altered by repositioning the footplate. The baseline condition served as the reference for analyzing parameter sensitivity in the computational model.

Comparison between experimental results and the modeled behaviors provided insights into the influence and sensitivity of each property. The variance accounted for (VAF) between the experimental trials and the VAF between modeled torques were compared to evaluate the validity of the model under different property adjustments. The findings presented in this paper enhance the understanding of the interactions between optimization models and physical systems, particularly regarding how specific properties influence the stability of neural and non-neural parameter quantification. By improving the understanding of these interactions, the study contributes to the development of a more reliable computational tool for assessing spasticity.

2 Method

2.1 Participants

Two young adults participated in the study presented in this paper. A 25-year-old female participant (P1), measuring 159 cm in height and weighing 65 kg, and a 29-year-old male participant (P2), measuring 180 cm in height and weighing 76 kg. Both participants gave written consent. Furthermore, the study was approved by the Human Research Ethics Committee of the TU Delft under application number 4216.

2.2 Instrumentation

Perturbations were applied using the Achilles system (MOOG FCS, Nieuw-Vennep, The Netherlands), which served as the robotic manipulator. EMG signals were recorded using the TMSi Porti7-8b8at system (TMSi BV., Oldenzaal, The Netherlands) with bipolar configuration. EMG data was collected from the gastrocnemius medialis (GM), gastrocnemius lateralis (GL), soleus (SOL), and tibialis anterior (TA) muscles. The bipolar electrodes were placed according to SENIAM standards [57, 58].

Torque, position, and EMG signal data were sampled at 2048 Hz. Postprocessing of the EMG signals involved three steps. First, the signals were bandpass filtered using a 3rd order Butterworth filter at 20 - 400 Hz. Second, the filtered signals were rectified. Third, the signals were lowpass filtered using a 3rd order Butterworth filter at 20 Hz. Finally, all data was down-sampled by a factor of 32 before being used for the parametric optimization model [12, 59].

2.3 Experimental Setup

Participants were seated in a car seat that could slide in the posterior-anterior direction, allowing the knee to be angled at 45 degrees, 0 degrees being full extension (see Figure 1).

The dominant foot of each participant was secured to the foothold using three Velcro straps. The rotational axis of the ankle was manually aligned with the rotational axis of the motor by adjusting the foothold. A computer screen was positioned in front of the participant to provide instructions, specifically asking them to relax their dominant ankle.

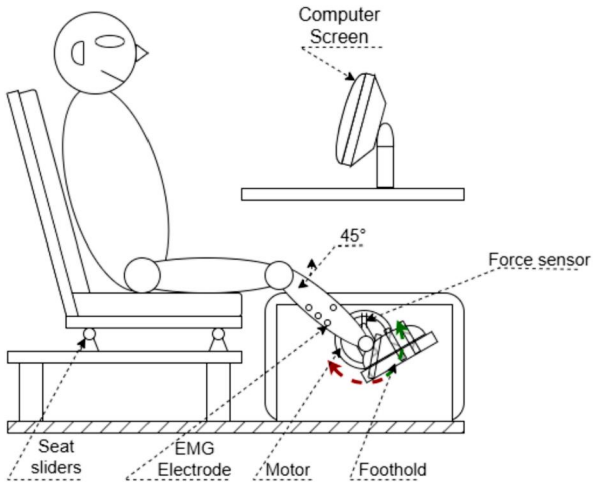

Figure 1: Experimental setup: Seat is adjustable in anterior-posterior direction. The motor of the Achilles robot applies 1 degree of freedom perturbations to the ankle: Plantarflexion (red) and dorsiflexion (green). The footplate can be adjusted in the toe-to-heel direction. A force sensor is attached between the foothold and the motor shaft. A computer screen was positioned in front of the participant.

2.4 Protocol

The protocol was designed to investigate the passive dynamic properties of the ankle joint. Perturbations were implemented to explore the mechanical behavior of the ankle, including its RoM, and to separately assess the effects of individual external factors such as adding a mass or stiffness and changing alignment. The passive RoM of the ankle was determined using a torque protocol adopted from Sloot et al. 2015 [47]. Incremental torque was applied until a threshold of 10 Nm plantarflexion or 15 Nm dorsiflexion was reached. For normalization purposes, 90% of the measured RoM was used as the maximum range for the trials.

Using position perturbations, each trial consisted of a preconditioning and an experimental phase (see Figure 2). The sinusoidal preconditioning was included to enhance trial consistency by mitigating the thixotropic phenomenon in the muscles [60]. During preconditioning, the foot was first positioned at the midpoint of the RoM using a RaH, followed by a sinusoidal perturbation spanning 80% of the RoM for fifteen seconds at a frequency of 0.3 Hz.

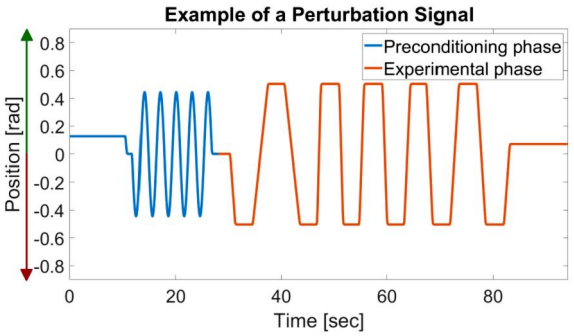

Figure 2: Example of a position perturbation profile, with an anti-thixotropic sinusoidal preconditioning phase (blue), and an experimental phase (orange). The experimental phase includes ramp-and-holds (RaH) to set, perturb, and reset the position. The RaHs that perturb consist of five velocities in randomized order and are in plantarflexed (red) and dorsiflexed (green) directions. 0 rad represents the midpoint of the range of motion of the participant.

The experimental phase consisted of RaHs at five velocities (20, 35, 50, 65, and 80 deg/s) in a randomized order. Each RaH had an amplitude of 90% of the RoM. The hold period, which also served as the rest period, lasted 2 seconds plus an additional random duration uniformly distributed between 0 and 0.5 seconds. This random duration was included to prevent participant anticipation effects.

The experimental phase from each trial had to be post-processed to compare the sections where the triceps surae were stretched. The data was segmented from 0.5 seconds before the stretch to the end of the hold period. To account for the added random duration, all sections were truncated to the shortest stretch duration at each velocity to enable averaging.

All trials were performed under seven conditions while the participant was asked to fully relax, with EMG measurements recorded throughout. The seven conditions were as follows:

- Baseline condition (**B**).
- Condition 'Added Mass 1' (**M1**).
- Condition 'Added Mass 2' (**M2**).
- Condition 'Added Stiffness 1' (**K1**).
- Condition 'Added Stiffness 2' (**K2**).
- Condition 'Changed Alignment 1' (**A1**).
- Condition 'Changed Alignment 2' (**A2**).

The baseline condition was performed without additional mass or stiffness and with an optimal alignment. Each condition was performed three times, except for condition A2, which was performed only twice due to a machine error. Variability between trials was measured using the variance accounted for (VAF) (see Formula 1).

$$VAF_{reps} = \left(1 - \frac{\sum(T_i - T_j)^2}{\sum(T_i)^2}\right) * 100\% \quad (1)$$

where T represents the torque of a trial.

An additional trial was performed under the baseline and alignment conditions to calculate the inertia, and thus the mass, of the foot and footplate combination. A multi-sine perturbation with an amplitude of 10% of the RoM, containing the frequencies 0.2, 0.5, 0.8, 8, 9, and 10 Hz, was applied for 360 seconds. The resulting data was analyzed using a fast Fourier transform, to generate an admittance plot and to calculate the eigenfrequency under the baseline and alignment conditions.

2.4.1 Mass Conditions

Two conditions involved adding a mass to the setup to measure the influence of the mass. In the conditions 'Added Mass 1' (M1) and 'Added Mass 2' (M2), a steel plate with dimensions of 190 x 139 mm and thicknesses of 1 mm and 2 mm, respectively, was attached to the bottom of the foothold (see Figure 3).Mass 1 and mass 2 weighed 0.162 kg and 0.410 kg, respectively. The masses were attached 20 mm from the footplate using 200 x 4.6 mm plastic cable ties.

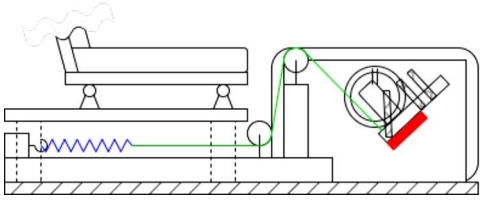

Figure 3: Spring and mass condition setup. For the spring conditions, an apparatus was placed under the seat. A metal wire (green) attaches a spring (blue) to the footplate. Two pulleys redirect the force direction of the spring to align with the calf muscles. For the mass conditions, a mass (red) is attached to the bottom of the footplate such that its moment arm is perpendicular to the footplate.

2.4.2 Spring Conditions

Two conditions with added stiffness were tested using springs to measure the influence of stiffness. In the conditions 'Added Spring 1' (K1) and 'Added Spring 2' (K2), a spring with stiffness coefficients of 144.3 N/m and 129.1 N/m, respectively, was attached to the heel side of the footplate (see Figure 3). The springs were secured to the footplate using a 2 mm thick metal wire. Additionally, two pulleys were used to align the force direction of the springs with the triceps surae muscles. The springs were placed under tension with the footplate positioned at the minimum of the RoM. The data for participant P2 for condition K1 was compromised due to a setup error and had to be discarded.

2.4.3 Alignment Conditions

Apart from the optimal alignment, two other alignments were tested to examine the influence of suboptimal ankle alignment. Optimal alignment of the rotational axes of the ankle and motor was achieved by minimizing knee movement. However, some translation of the knee was inevitable due to the complex nature of the ankle joint. The footplate offered three distinct alignment options, spaced 5 mm apart, allowing for a total modification of 10 mm in the heel-to-toe direction. The alignment option with the least knee movement was selected for all but the alignment condition trial. For participant P2, condition 'Alignment 1' (A1) was misaligned by 5 mm, and condition 'Alignment 2' (A2) was misaligned by 10 mm from

the baseline condition. The alignment conditions were not tested on participant P1 due to unforeseen testing delays.

2.5 Parametric Optimization Model

2.5.1 Neuromuscular Model

The model used in this study was initially developed by Vlugt et al. [12]. Subsequently, multiple parties contributed to improving the model by modifying the calculations surrounding the foot and footplate combination and adding parameters such as misalignment, tonicity, and torque bias [11, 46–51]. The model consists of Hill-type muscle models and uses EMG data of the GM, SOL, GL, and TA muscles, along with position data from the ankle, as input. The model outputs a total torque and 23 optimized parameters (see Table 1).

The total torque is composed of passive elastic, active muscle, gravitational, inertial, and misalignment torques (see Formulas 2-6). The misalignment torque accounts for an additional torque caused by imperfect alignment of the ankle joint. The torques were calculated as follows:

$$T_{elastic} = exp(k * (x - x0)) * r \quad (2)$$

$$T_{active} = cl * cv * A * r \quad (3)$$

$$T_{gravity} = m * g * Pcom_{FP,G} + T_{bias} \quad (4)$$

$$T_{inertia} = I * \ddot{th} \quad (5)$$

$$T_{misalign} = F_{leg} * d_{misalign} * cos(th_{fp}) \quad (6)$$

where $T_{elastic}$, T_{active}, $T_{gravity}$, $T_{inertia}$, and $T_{misalign}$ are the elastic, active muscle, gravitational, inertial, and misalignment torque, respectively. With k, the stiffness coefficient, x the current muscle length, and $x0$ the slack length of either the TA or the TS muscles. Additionally, cl represents the force-length relationship, cv the force-velocity relationship, and H_{act} the second-order activation dynamics. Other parameters include m for the mass of the foot and footplate, g for the gravitational constant, $Pcom_{FP,G}$ for the center of mass of the foot in the global coordinate system (CS), and T_{bias} for the torque bias. Furthermore, I represents the inertia of the foot and footplate, and $\ddot{th}$ is the rotational acceleration. The misalignment torque, $T_{misalign}$, is calculated using F_{leg} the force exerted by the leg on the footplate, $d_{misalign}$ the misalignment distance, and th_{fp} the angle of the footplate.

The second-order activation dynamics, represented by H_{act} is as follows:

$$H_{act}(s) = \frac{\omega_0^2}{s^2 + 2\beta\omega_0 s + \omega_0^2} \quad (7)$$

where ω_0 is the natural frequency, and β is the relative damping coefficient. This model characterizes the dynamic response of the activation signal to the neural excitation.

2.5.2 Optimization

Using the neuromuscular model, an optimization was conducted with the non-linear least squares method employing the trust-region-reflective algorithm. The objective of the optimization was to minimize the difference between the measured (T) and the total modeled torque ($\hat{T}$) (see Figure 4).

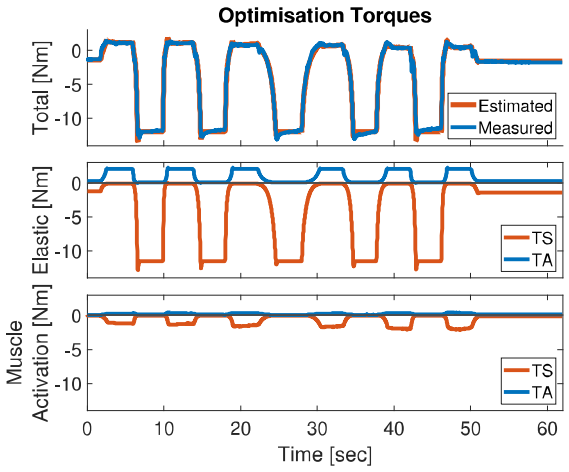

Figure 4: Optimized torques. Top panel: estimated (orange dashed) and measured (blue) total torque. The difference between the estimated and measured total torque makes up the objective function of the optimization. Middle panel: elastic torque of the triceps surae (TS) (orange) and tibialis anterior (TA) (blue dashed). Bottom panel: muscle active torque of the TS (orange) and TA (blue dashed).

Only the experimental phase of each trial was used for the optimization to exclude the shift in the thixotropic effects of the muscles. Lower and upper bounds constrained all parameters, ensuring realistic values, and no pa-

Table 1: Parameters being optimized with their descriptions, units, starting values, and lower and upper bound values.

Parameter	Description	Unit	Starting value	Lower bound	Upper bound
m	mass foot+footplate	kg	3	2	5
k_{tri}	Stiffness coefficient TS	m^{-1}	300	100	400
k_{tib}	Stiffness coefficient TA	m^{-1}	170	40	800
$x0_{tri}$	Slacklength TS	m	0.035	0.001	0.08
$x0_{tib}$	Slacklength TA	m	0.05	0.02	0.13
τ_{rel}	Relaxation time constant	s	2	0.01	10
k_{rel}	Relaxation factor	-	0.1	0.015	3
g1	EMG weight factor TA	N/V	1	0	5000
g2	EMG weight factor GL	N/V	1	0	5000
g3	EMG weight factor SOL	N/V	1	0	5000
g4	EMG weight factor GM	N/V	1	0	5000
$L0_{tri}$	Optimal muscle length TS	m	0.05	0.02	0.2
$L0_{tib}$	Optimal muscle length TA	m	0.09	0.07	0.13
f0	Cut-off frequency activation filter	Hz	1	2	20
β	Relatie damping coefficient activation filter	-	1	0.5	8
$T_{misalign}$	Misalignment ankle joint	m	0	-0.005	0.005
$FPcom_{dx}$	x pos CoM FP in local c.s. origin in Achilles joint	m	0	-0.01	0.1
$FPcom_{dy}$	y pos CoM FP in local c.s. origin in Achilles joint	m	0	-0.08	-0.05
Tbias	Bias torque	Nm	0	-1.6	1.5
$Tonic_{tib}$	Noise of TA	V	0.5	0	1
$Tonic_{tri1}$	Noise of GL	V	0.5	0	1
$Tonic_{tri2}$	Noise of SOL	V	0.5	0	1
$Tonic_{tri3}$	Noise of GM	V	0.5	0	1

rameters were fixed during the optimization (see Table 1).

The optimization process was set to a maximum of 100 iterations and allowed up to 15,000 function evaluations. It employed a step tolerance of 1×10^{-9} and a function tolerance of 1×10^{-29}. To reduce the likelihood of converging to a local minimum, the optimization was initialized from ten different random starting conditions, with the randomness uniformly distributed between the lower and upper bounds.

The validity of the optimization was assessed using two metrics, the VAF and the root mean square error (RMSE) (see Formulas 8, 9). The VAF quantifies how much of the variance in the measured torque is explained by the modeled torque, with 100% indicating a perfect fit. Likewise, the RMSE reports the deviation between measured and modeled torque, where an error of 0 signifies a perfect fit.

$$VAF_{model} = \left(1 - \frac{\sum(T - \hat{T})^2}{\sum(T)^2}\right) * 100\% \quad (8)$$

$$RMSE = \sqrt{\frac{\sum_1^n (T - \hat{T})^2}{n}} \quad (9)$$

where T represents the measured torque, $\hat{T}$ represents the modeled torque, and n is the total number of measured samples.

2.5.3 Model Sensitivity Analysis

Using the baseline conditions of the participants, a model sensitivity analysis was performed by varying one parameter at a time and rerunning the model. The influence of

each parameter was evaluated by comparing the resulting torques. The significance of the effect of each parameter was assessed qualitatively by examining the magnitude of change in the torque profiles. To account for differences in the sensitivity of the model to each parameter, the parameters were varied by different magnitudes. The mass was adjusted by ±50%, the stiffness by ±2%, and the misalignment by ±100%.

3 Results

3.1 Experimental data

Position and torque data were recorded throughout the trials, with the RoM values measured at the outset. Participants P1 and P2 had a RoM of 1.119 and 0.916 rad, respectively. Notably, participant P2 reported having tight Achilles tendons. The RoM values resulted in RaH amplitudes of 1.007 and 0.824 rad for participants P1 and P2, respectively.

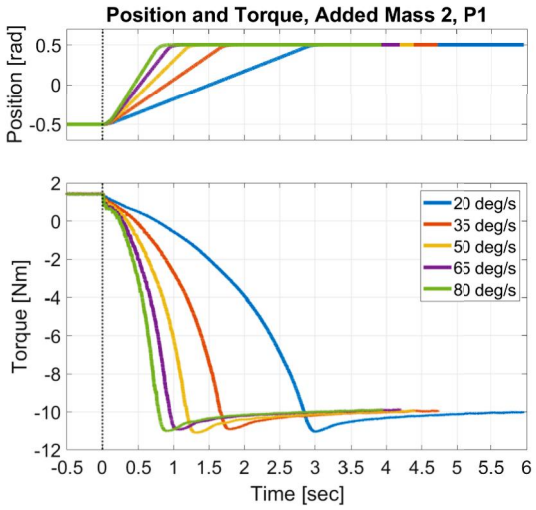

Figure 5: Means of ramp-and-holds (RaH) of trial 'Mass 2' of participant P1 for five different velocities: 20 deg/s (blue), 35 deg/s (orange), 50 deg/s (yellow), 65 deg/s (purple), and 80 deg/s (green). RaHs are from a plantarflexed to a dorsiflexed position. Top panel: Means of position profiles per velocity. Bottom panel: Means of torque profiles per velocity.

The recorded position and torque data revealed distinct mean position and torque profiles across the five velocities tested (see Figure 5). A relatively consistent maximum torque of approximately 11 Nm was achieved to attain the desired velocity and stretch amplitude.

Excluding the trials for condition A2, mean torque values were calculated from three repeated measurements for each condition. The three repeated measurements revealed variations in the absolute maximum torques and the timing of the peak values (see Figure 6).

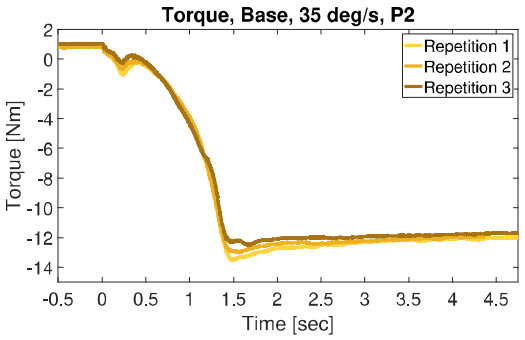

Figure 6: Ramp-and-holds (RaHs) of base condition at 35 deg/s of participant P2. RaHs are from a plantarflexed to a dorsiflexed position. Each repetition is shown separately.

The VAF_{rep} metric was used to assess variability between trials. Across conditions, the trials demonstrated excellent consistency, with VAF_{rep} values exceeding 99% (see Table 2). Even the outlier condition M1 for participant P1 maintained a VAF value of 92.09%.

Table 2: Variance accounted for and root mean square error values between trials to indicate the repeatability of trials for all conditions: Base (B), added mass 1 (M1), added mass 2 (M2), added spring 1 (K1), added spring 2 (K2), alignment 1 (A1), and alignment 2 (A2).

Condition	VAF [%]	
	P1	P2
Base	99.83	99.86
Mass 1	92.09	99.77
Mass 2	99.97	99.38
Spring 1	99.95	-
Spring 2	99.92	99.93
Align 1	-	99.76
Align 2	-	99.86

The means for each condition were grouped into graphs based on velocity to facilitate comparison of effects (see Figure 7). For conditions M1, M2, and the baseline, no clear distinctions

were observed before the stretch. However, as the ankle rotated toward a dorsiflexed position, differences became apparent and progressively larger. During the hold phase, a distinct increase in torque was observed with the addition of mass, with the heavier mass (M2) resulting in a greater increase. For participant P1, the difference between the baseline and M1 conditions diminished with faster stretch velocities (see Appendix B). Conversely, for participant P2, the differences between conditions were significantly smaller and, in some cases, negligible (see Appendix C).

Adding a spring to the setup affected the torque before, during, and after the stretch. Before the stretch, an offset was observed when comparing the baseline condition to the spring conditions for participant P1. As the ankle moved toward a dorsiflexed position, the difference in torque increased and became most pronounced during the hold phase.

Adjusting the alignment showed minimal effects overall. For all stretches except those at 80 deg/s, condition A1 exhibited the largest negative torque at the end of the stretch, while condition A2 exhibited the smallest negative torque (see Appendix C). Notably, the torque in condition A2 also started at a lower value.

3.2 Model Sensitivity Analysis

The results of the model sensitivity analysis revealed varying influences of the mass, stiffness, and alignment parameters on the modeled torque (see Figure 8). Changes in mass affected the torque in the stationary phases of the RaHs. A decrease in mass shifted the torque towards more positive values, thereby decreasing the absolute maximum torque. Conversely, an increase in mass shifted the torque toward more negative values, resulting in a higher absolute maximum torque.

The model exhibited the greatest sensitivity to changes in TS stiffness. Although the TS stiffness was adjusted with the smallest percentage, it produced the largest absolute difference in torque. These changes were confined to the hold phases, during which the TS was stretched.

Adjustments to the alignment parameter had minimal impact on the modeled torque, even with the largest percentage changes. Reducing the misalignment decreased torque during the hold phases when either the TS or TA was stretched. Conversely, increasing the misalignment resulted in a torque increase in all stationary phases.

3.3 VAF & RMSE

The VAF and RMSE metrics were calculated to evaluate repeatability between trials and to analyze the influence of mass, stiffness, and alignment in the model sensitivity analysis (see Figure 9). In the model sensitivity analysis, changes in TS stiffness had the greatest impact on the model, while changes in misalignment had the smallest effect. The VAF_{rep} values were all close to 100%, except for the outlier condition M1 of participant P1.

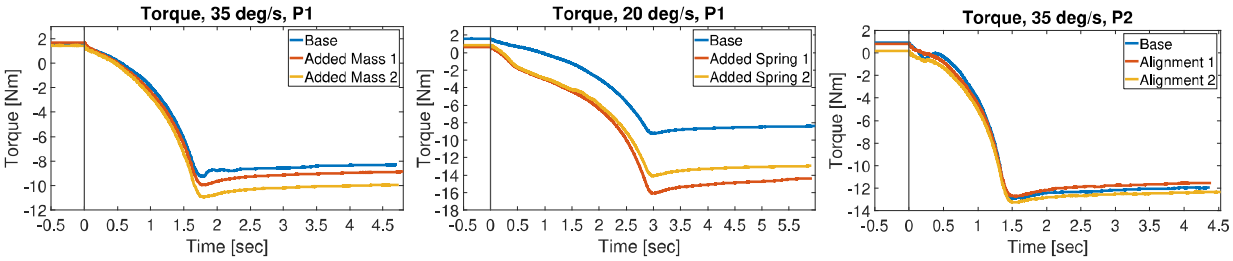

Figure 7: Means of torque profiles. Ramp-and-hold from plantarflexed to dorsiflexed position starts at 0 sec. Left panel: conditions 'Base' (blue), 'Added Mass 1' (orange), and 'Added Mass 2' (yellow) at 35 deg/s of participant P1. Middle panel: Conditions 'Base' (blue), 'Added Spring 1' (orange), and 'Added Spring 2' (yellow) at 20 deg/s of participant P1. Left panel: Conditions 'Base' (blue), 'Alignment 1' (orange), and 'Alignment 2' (yellow) at 35 deg/s of participant P2.

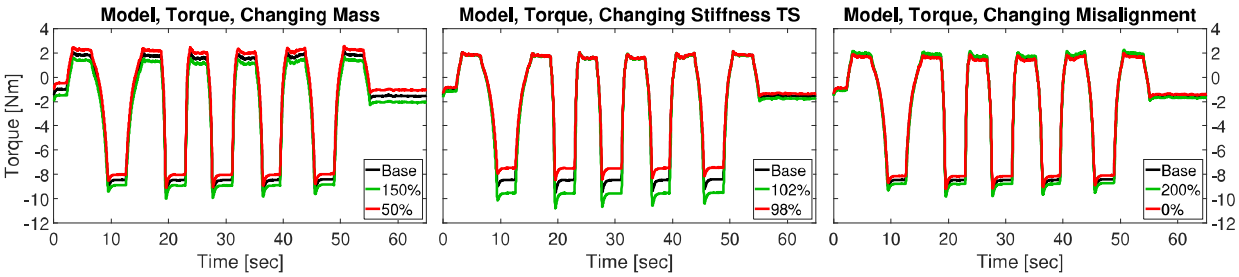

Figure 8: Estimated torque outputs of the sensitivity analysis of the model. Left panel: The mass parameter is tested at base or 100% (black), 150% (green), and 50% (red). Middle panel: The triceps surae stiffness parameter is tested at base or 100% (black), 102% (green), and 98% (red). Left panel: The misalignment parameter is tested at base or 100% (black), 200% (green), and 0% (red).

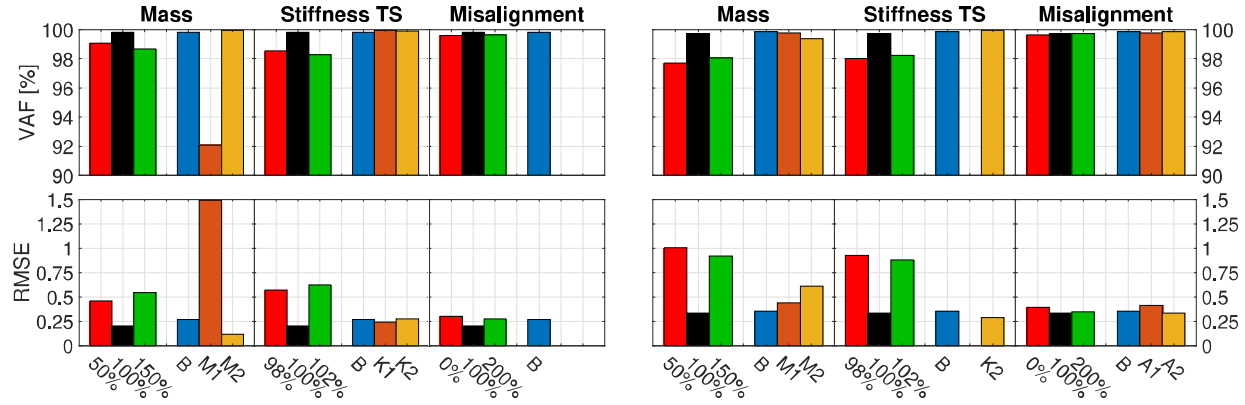

Figure 9: Variance Accounted For (VAF) and Root Mean Square Error (RMSE) of the model limited sensitivity analysis (red, black, and green) and across repetitions of each experimental condition (blue, orange, and yellow). The panels are grouped per six and correspond to participants P1 (left six panels) and P2 (right six panels). Left panels of each group: Mass parameter and conditions 'Added Mass 1' (M1) and 'Added Mass 2' (M2). Middle panels of each group: Stiffness triceps surae (TS) parameter and conditions 'Added Spring 1' and 'Added Spring 2' (K2). Right panels of each group: Misalignment parameter and experimental trials 'Alignment 1' (A1) and 'Alignment Mass 2' (A2). Excluding the outlier, condition M1 of participant P1, the lowest VAF and highest RMSE observed were 99.38%, and 0.6062 respectively.

3.4 Optimization

Of the 23 optimized parameters, only five are discussed in detail (see Figure 10). Parameters related to muscle activation were excluded, as participants remained fully relaxed during all trials. Similarly, the misalignment parameter and associated conditions were omitted due to their minimal influence. The minimal effect of the alignment was also reflected in the inertia tests, where the base alignment and alignment A1 were compared (see Appendix A). Furthermore, the decrease in VAF_{rcp} for the alignment conditions exceeded the effects of alignment changes, further justifying their exclusion. The analysis focuses on parameters associated with calculating elastic torque and the remaining parameters related to passive torques. These parameters were selected based on their relevance to the study objectives and their observed impact on the modeled torque.

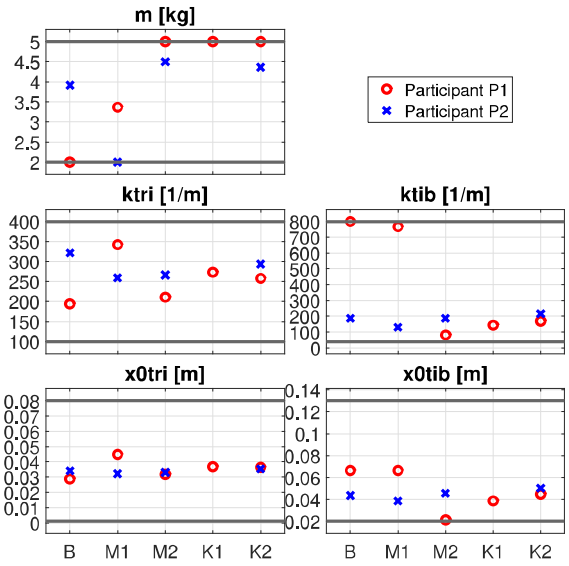

Figure 10: Resulting optimized parameter values for participants P1 and P2. Each panel contains the values for trial 'Base' (B), 'Added Mass 1' (M1), 'Added Mass 2' (M2), 'Added Spring 1' (K1), and 'Added Spring 2' (K2). Top left panel: mass values. Middle left panel: stiffness triceps surae (TS). Middle right panel: stiffness tibialis anterior (TA). Bottom left panel: slack length TS. Bottom right panel: slack length TA.

For participant P1, a clear increase in the mass parameter is observed when either a mass or spring is added. Conditions M2 and K2 approach the upper bound of the mass parameter range, with condition K1 reaching it. Comparing the spring conditions to the baseline condition, a proportional increase in the stiffness of the TS is evident. An increase in TS stiffness is also observed for condition M2. However, condition M1 shows an unexpectedly large increase in TS stiffness, which deviates from the overall trend. The stiffness of the TA shows unusual behavior in the baseline condition and condition M1, with the baseline condition reaching the upper bound and condition M1 nearing it.

For participant P2, conditions M2 and K2 exhibit increases in the mass parameter, while condition M1 shows an unexpected decrease. Compared to the baseline, a general decrease in TS stiffness is observed across the non-baseline conditions. In contrast, the stiffness of the TA remains largely unchanged across all conditions.

The slack lengths of the TS remain consistent across all conditions for both participants. For the TA, the slack length is consistent for participant P2. For participant P1, the TA slack length is similar only between the baseline condition and condition M1.

4 Discussion

4.1 Experimental Data

All torque profiles displayed the characteristic exponential shape typically associated with ankle torque behavior during passive stretching [12, 46, 61]. Each curve also exhibited an overshoot, indicating a transient torque peak before stabilizing. The overshoot may reflect the dynamic response of the ankle joint to the imposed perturbation [62–64]. The variability between repetitions underscores the importance of averaging repeated trials to ensure robust data analysis.

4.1.1 Mass Conditions

Comparing the mass and baseline conditions revealed unexpected torque behavior. Before a stretch, as the footplate was parallel to the ground, the difference in torque should be negligible. In this configuration, the added mass exerts a force on the footplate in line with the arm connecting it to the motor. In other words,

the added mass had no moment arm, pulling perpendicular to the direction of motion, and thus should not require additional torque while stationary. As the ankle was dorsiflexed further, the moment arm of the mass increased proportionally, and the required torque should increase accordingly. In the dorsiflexed configuration, the mass reached its largest moment arm and should require the greatest torque to keep the footplate stationary.

For participant P1, who had a lighter foot, the effects of adding mass were relatively larger, as expected. The differences in torque between the baseline condition and condition M2 were consistent. However, while condition M1 showed a proportional increase in torque at lower velocities, the torque became more similar to the baseline condition at higher stretch velocities. Condition M1 was also an outlier in the VAF_{rep} values, showing greater variance between trials. The torque data from the first repetition of condition M1 had an offset towards more positive values, shifting the torque data closer to the baseline condition during averaging. This inconsistency resulted in greater variance and, consequently, a lower VAF_{rep} value.

For participant P2, who had a heavier foot, the relative differences between the baseline and mass conditions were smaller, as expected. However, the absolute differences should have stayed consistent. At 20 and 80 deg/s, the torque differences between the baseline condition and condition M1 were consistent. Larger differences were expected at 35, 50, and 65 deg/s. For condition M2, the differences were smaller than anticipated, with the required torque at 65 deg/s even being smaller than in the baseline condition (see Appendix B). Notably, the torque profile at 65 deg/s was an outlier, as the torque during the hold phase differed from the other velocities. Furthermore, condition M2 had the lowest VAF_{rep} compared to conditions B and M1, indicating unreliable data.

The unexpected behavior in condition M2 for participant P2 possibly resulted from measurement variability or experimental inconsistencies. One possible explanation is that the participant shifted positions during the attachment of the second mass. If the participant sat further back, they could have exerted less force with their leg on the footplate. Additionally, the participant may not have been fully relaxed during one trial at 65 deg/s, inadvertently moving with the robotic manipulator. The heavier foot of the participant may have introduced greater inertia, reducing the sensitivity of the torque readings to the added mass, particularly at higher velocities.

Finally, the discrepancies observed in both participants suggest a potential non-linear relationship between velocity and torque requirements when mass is added. This finding may reflect how biomechanical factors, such as muscle activation or joint stiffness, adapt differently to added mass at varying speeds [65].

4.1.2 Spring Conditions

The spring conditions demonstrated the most consistent and predictable torque behavior among the tested conditions. The stiffness of the ankle resulted in a non-linear, exponential torque shape. The springs are expected to produce a linear increase in torque across the RoM. Because the springs were placed under tension with the footplate positioned at the minimum of the RoM, a shift in torque was visible just before the stretch began. The torque difference increased as the ankle was manipulated toward a dorsiflexed position.

For participant P1, the behavior aligned with expectations. A degree of torque shift was observed before the stretch began, caused by the weight of the spring and the tension exerted on the footplate. Comparing the spring conditions, the stiffer spring, added spring 1, showed a greater increase in torque as the ankle was stretched.

Notably, for all velocities except 20 deg/s, during the dynamic phase of the stretch, a narrowing of the torque profiles was observed between the baseline and spring conditions. This narrowing may be due to a change in joint angles resulting from a positional shift by the participant between the baseline and spring conditions. The change in joint angles resulted in a change in the slack length of the muscles, which affected the exponential torque curve of the ankle [46, 47, 66–68]. Although the spring contraption was in place before the baseline trials to minimize interference between trials, it is

possible that the participant repositioned while the metal wire was being attached to the footplate, as this step occurred between the baseline and spring trials. Importantly, no such difference was observed between the spring trials, as the springs were replaced without requiring proximity to the participant.

For participant P2, similar behavior to participant P1 was observed. The torque difference between the baseline and spring conditions was smaller before the start of the stretch compared to participant P1, likely due to lower initial spring tension. The same narrowing of the torque profiles was visible. Since the protocol was identical for both participants, the likely explanation is a change in joint angles, and thus slack lengths, caused by a positional shift to accommodate the metal wire.

The findings for both participants suggest that while the spring conditions exhibit consistent behavior overall, procedural factors, such as the attachment of the metal wire, can introduce variability in the torque profiles. The narrowing of the torque profiles during the stretch phase is likely due to participant-specific factors, such as changes in joint angles. Additionally, the lack of change in torque profiles between spring trials supports the robustness of the spring contraption. For participant P2, the reduced torque difference before the start of the stretch underscores the importance of precise and consistent spring tensioning during setup to ensure comparable conditions.

Overall, the results demonstrate that the spring conditions produce consistent torque profiles. However, small procedural inconsistencies, such as variations in initial tension and participant joint angles, can influence the torque profiles. These findings highlight the need for meticulous control of setup conditions to minimize variability and improve the reliability of the experimental outcomes.

4.2 Model

Discrepancies arise when comparing the torques of the experimental conditions with the model sensitivity analysis. Firstly, the focus is on the mass. In the model sensitivity analysis, altering the mass parameter consistently affected the stationary phases, regardless of the position of the ankle. However, in the experimental data, the increased mass did not affect torque when the foot was in the plantarflexed position, parallel to the ground. The effect of the mass on the torque grew as the horizontal moment arm of the mass to the rotational axis of the motor increased. This observation indicates that the model does not fully account for the physical characteristics of the Achilles robot.

For the stiffness, the torques of the experimental data and model sensitivity analysis showed similarities. In both cases, during the hold phase of the TS stretch, torque increased to keep the foothold stationary. However, during the stationary phase where the TA is stretched, the model showed no effect from a changed stiffness. In contrast, the experimental data revealed a difference, as the spring exerted force in this phase. Additionally, in the dynamic phase of the perturbation, changing the TS stiffness parameter did not affect the torque, whereas adding a spring in the experimental setup did. Although the TS was not in a stretched position from plantarflexion to the neutral position, it was still being lengthened. A difference might have been observed if the participant had contracted their TS. From the neutral to dorsiflexed position, the TS was stretched, and with increased stiffness, a change in torque was expected. Tensioning the spring in a neutral ankle position could potentially align the experimental data more closely with the model sensitivity analysis graphs.

In summary, the discrepancies observed in the effect of mass on the torque profiles between the experimental data and the model sensitivity analysis highlight the limitations of the current model in capturing the physical nuances of the Achilles. Additionally, the effects of the added stiffness on the torque profiles between the experimental data and the model sensitivity analysis highlight the limitations of the physical nuances of the experimental setup.

4.2.1 VAF & RMSE

The analysis of the VAF_{model} and RMSE values reinforces that each parameter exerts a different magnitude of influence, consistent with the experimental data. Among the parameters, the stiffness of the TS had the greatest impact,

followed by the mass parameter. Comparison of the change in VAF_{rep} with the change in VAF_{model}, shows the significance of the mass and stiffness parameters. Changes in both parameters result in greater variance than the variance caused by trial repetitions. Specifically, the TS stiffness emerges as the most sensitive parameter for accurately modeling the behavior of the system.

4.3 Optimization

The five parameters presented in 10 were optimized using the parametric optimization model and assessed to determine whether the model captures changes caused by adding a mass or spring to the experimental setup. The conditions M1, M2, K1, and K2 were compared to the baseline condition to identify trends in how the optimized parameters responded to these changes.

For Participant 1, the TS stiffness consistently increased across all conditions, underscoring its dominant role in managing increased torque demands. Conversely, TA stiffness decreased significantly, particularly in condition M2. The slack lengths varied, with increased TS and decreased TA slack lengths compared to the baseline condition.

Adding a mass during the experiments increased the torque during the hold phases while the TS was stretched. The optimization accounted for this by increasing both the mass and TS stiffness parameters, indicating that the optimization captured the added mass. The likely reason for increasing the TS stiffness parameter is its strong influence on torque during the stationary phases of the perturbation. The unexpectedly large increase in TS stiffness for condition M1 may reflect variability also observed in the VAF_{rep}. For condition M2, the reduction in TA stiffness suggests a diminished contribution of the TA, potentially as an optimization adjustment to reduce the modeled torque during the hold phase when the TA was stretched.

Adding a spring introduced a non-uniform increase in torque across the perturbation. The model addressed the increased torque during the hold phases while the TS was stretched by increasing the TS stiffness parameter, suggesting that the optimization captured the increased stiffness caused by the spring. Conversely, the reduction in torque during the hold phases while the TA was stretched was managed by decreasing TA stiffness. This adjustment was more pronounced for the stiffer spring condition K1. Slack lengths were likely adjusted to account for torque alterations during the dynamic phases of the perturbation.

For Participant P2, adjustments in the stiffness and slack length parameters were more subtle and consistent compared to Participant 1. Participant P2 exhibited a reduced role of the TS and an increased role of the TA across conditions, with minimal changes in slack lengths. The added mass did not have the same effect on the parameters of participant P2 as it did on Participant P1. The inconsistent effects the mass had on the torque profiles of participant P2, hindered the ability of the computer model to adapt the parameters effectively. An increase in the mass parameter is still present for condition M2, while condition M1 unexpectedly showed a decrease. The TS stiffness parameter decreased in both mass conditions, suggesting a reduced contribution of the TS. Relatively to participant P1, the TA stiffness parameter remained unchanged, likely because the torque during the hold phases while the TA was stretched was inconsistent for the mass conditions. Slack lengths remained consistent, reflecting the near-identical dynamic phases of the perturbations.

For condition K2, the torque increased during both the dynamic phases and stationary phases while the TS was stretched. The optimization accommodated this by increasing the mass parameter compared to the baseline condition. The hold phases during which the TA was stretched showed minimal torque differences, explaining the consistency in the TA stiffness parameter. However, contrary to expectations, TS stiffness did not increase. Slack lengths for both TS and TA increased slightly, likely reflecting adjustments for torque differences during the dynamic phases.

4.3.1 VAF & RMSE

Examining the VAF_{model} and RMSE values revealed that changes in TS stiffness had a significantly greater influence on the modeled torque compared to changes in mass. Due to

this disproportionate influence, the optimization likely adjusts TS stiffness as the primary parameter to align the modeled and experimental torque. Consequently, the mass parameter, which has a smaller effect on torque, exhibits greater variability in parameter estimation, as the stiffness compensates for differences caused by mass changes. This behavior may explain why the mass parameter frequently reaches its lower or upper bounds.

4.4 Limitations

This study faced several limitations that impacted the results and their generalizability. Firstly, the limited participant pool. Due to machine error, the number of participants was restricted to two, significantly reducing the generalizability of the findings to a broader population.

Secondly, alignment adjustments. The experimental setup required detaching and reattaching the foothold to adjust alignment, which likely altered the position of the participant and introduced variability. Alignment adjustments were restricted to the toe-to-heel direction in the sagittal plane, with no capability for modifying proximal-distal alignment, potentially reducing the precision of the setup.

Thirdly, seat movement constraints. The seat could only be adjusted backward and forward, with no capability for adjustments in the frontal plane. This limitation restricted the ability to modify hip joint angles. Additionally, ankle rotations in the eversion-inversion direction were constrained.

Fourthly, the process of changing added masses. Adjusting the masses required manually handling the footplate, which may have inadvertently altered the joint angles of a participant, introducing additional variability into the experimental conditions.

Fifthly, attaching springs to the foothold. While springs could be interchanged without disturbing the participants, attaching the metal wire connecting the spring to the foothold before initiating the spring conditions required physical proximity by the researcher. This proximity may have unintentionally affected the joint angles of a participant.

Sixthly, the information sheet containing details about the springs was unavailable. Characteristics of the springs were assessed by hand, possibly resulting in less accurate measures of the springs and limited information about their preload. This limited information may have affected the torque profiles in unexpected ways.

Lastly, absence of precise real-time feedback on joint angles. The setup lacked mechanisms for precise, real-time monitoring and adjustment of joint angles, such as motion capture. This limitation likely contributed to variability caused by the processes described in the fourth and fifth limitations, as visual observation was the sole method for confirming participant positioning.

Addressing these limitations in future studies, such as by increasing the participant pool, improving setup processes, and incorporating real-time joint angle monitoring, could enhance the reliability and generalizability of the findings.

5 Conclusion

A sensitivity analysis was performed both experimentally on participants and digitally on a computer model. The current computer model does not fully capture the physical nuances of the experimental setup. Specifically, it does not incorporate the correct moment arm of the mass or fully capture the effects of stiffness during the dynamic phases of the perturbations. These limitations should be further investigated, particularly with a revised setup for the spring conditions. While the model correctly represents the alignment parameter, its effects are less pronounced than the variability observed between trials. Therefore, optimizing the alignment parameter is unlikely to improve the estimate.

Overall, the comparison between the experimental data and the model sensitivity analysis demonstrated that while the model successfully captures broad trends in the influences of the parameters on torque, refinements are required to better represent the detailed effects of mass and stiffness changes.

5.1 Recommendations

The findings emphasize the need for further refinement of the computer model. Specifically, incorporating detailed physical characteristics of the robotic manipulator, such as its moment arm, could enhance the predictive capabilities of the model and ensure closer similarity with real-world dynamics.

While the model provides a controlled framework, real-world complexities, such as variations in the joint configuration of a participant, can influence the outcomes. Future iterations of the protocol should incorporate strategies to ensure a more consistent alignment of the joint angles of a participant. These could include adding physical support structures, using markers, or integrating equipment for continuous measurement of joint angles. Furthermore, the preload of the springs requires further investigation. While 5% of the RoM of a participant was used to mitigate the non-linear effects of the preload, further analysis is needed to determine whether this fully eliminated those non-linear effects.

Regarding the optimization process, the large number of parameters suggests optimizing the 23 parameters in distinct steps. For instance, the mass could be determined through a test similar to the inertia test, using the eigenfrequency and impedance of the system to calculate the mass. Similarly, EMG parameters could be determined independently by performing an MVC test and aligning the EMG weight factors based on the resulting data. Determining and locking these parameters before running the full optimization would reduce the interdependence between parameters, simplifying the process and improving the accuracy of the results.

References

[1] William Barry McKay, William Mark Sweatman, and Edelle C. Field-Fote. The experience of spasticity after spinal cord injury: perceived characteristics and impact on daily life. *Spinal Cord*, 56(5):478–486, 2018. ISSN 1476-5624. doi: 10.1038/s41393-017-0038-y. URL https://doi.org/10.1038/s41393-017-0038-y.

[2] Dana Frisch and Michael E. Msall. Health, functioning, and participation of adolescents and adults with cerebral palsy: A review of outcomes research. *Developmental Disabilities Research Reviews*, 18(1):84–94, 2013. doi: https://doi.org/10.1002/ddrr.1131. URL https://onlinelibrary.wiley.com/doi/abs/10.1002/ddrr.1131.

[3] Rozina H Bhimani, Cynthia Peden McAlpine, and Susan J Henly. Understanding spasticity from patients' perspectives over time. *Journal of advanced nursing*, 68(11):2504–2514, 2012. doi: 10.1111/j.1365-2648.2012.05949.x. URL https://onlinelibrary.wiley.com/doi/full/10.1111/j.1365-2648.2012.05949.x?

[4] Nathaniel Larbi Andah. Access to healthcare services among children with cerebral palsy in the greater accra region of ghana. In Pinar Kuru Bektaşoğlu, editor, *Cerebral Palsy*, chapter 6. IntechOpen, Rijeka, 2023. doi: 10.5772/intechopen.106684. URL https://doi.org/10.5772/intechopen.106684.

[5] Grace Warner, Johanne Desrosiers, Tanya Packer, and Robin Stadnyk. Factors affecting ability and satisfaction with social roles in persons with neurological conditions: The importance of mobility and stigma. *British Journal of Occupational Therapy*, 81(4):207–217, 2018. doi: 10.1177/0308022617743695. URL https://doi.org/10.1177/0308022617743695.

[6] Schinwelski M.J., Sitek E.J., Waż P, and Sławek J.W. Prevalence and predictors of post-stroke spasticity and its impact on daily living and quality of life. *Neurologia i neurochirurgia polska*, 53(6):449–457, 2019. doi: 10.5603/PJNNS.a2019.0067.

[7] Şahin S, Köse B, Aran O.T., Bahadır Ağce Z, and Kayıhan H. The effects of virtual reality on motor functions and daily life activities in unilateral spastic cerebral palsy: A single-blind randomized controlled trial. *Games for health journal*, pages 45–52, 2020. ISSN 2161-7856. doi: 10.1089/g4h.2019.0020.

[8] Corbetta D, Sirtori V, Castellini G, Moja L, and Gatti R. Constraint-induced movement therapy for upper extremities in people with stroke. *The Cochrane database of systematic reviews*, 2015. ISSN 1361-6137. doi: 10.1002/14651858.CD004433.pub3.

[9] Khan F, Amatya B, Bensmail D, and Yelnik A. Non-pharmacological interventions for spasticity in adults: An overview of systematic reviews. *Annals of physical and rehabilitation medicine*, 62(4):265–273, 2019. ISSN 1877-0665. doi: 10.1016/j.rehab.2017.10.001.

[10] J.W. Lance. The control of muscle tone, reflexes, and movement: Robert wartenbeg lecture. *Neurology*, 1980. doi: 10.1212/wnl.30.12.1303.

[11] K.L. De Gooijer van de Groep, E. de Vlugt, J.H. de Groot, H.C. van der Heijden-Maessen, D.H. Wielheesen, R.S. van Wijlen-Hempel, and C.G. Meskers. Differentiation between non-neural and neural contributors to ankle joint stiffness in cerebral palsy. *Journal of NeuroEngineering and Rehabilitation*, 2013. doi: 10.1186/1743-0003-10-81.

[12] E. de Vlugt, J.H. de Groot, K.E. Schenkeveld, J.H. Arendzen, F.C. van der Helm, and C.G. Meskers. The relation between neuromechanical parameters and ashworth score in stroke patients. *Journal of NeuroEngineering and Rehabilitation*, 2010. doi: 10.1186/1743-0003-7-35.

[13] A.J. Starsky, S.G. Sangani, J.R. McGuire, B. Logan, and B.D. Schmit. Reliability of biomechanical spasticity measurements at the elbow of people poststroke. *Archives of Physical Medicine and Rehabilitation*, 2005. doi: 10.1016/j.apmr.2005.03.015.

[14] Lizeth H. Sloot, Guido Weide, Marjolein M. van der Krogt, Kaat Desloovere, Jaap Harlaar, Annemieke I. Buizer, and Lynn Bar-On. Applying stretch to evoke hyperreflexia in spasticity testing: Velocity vs. acceleration. *Frontiers in Bioengineering and Biotechnology*, 8, 2021. doi: 10.3389/fbioe.2020.591004.

[15] Yi-Ning Wu, Yupeng Ren, Ashlee Goldsmith, Deborah Gaebler, Shu Q Liu, and Li-Qun Zhang. Characterization of spasticity in cerebral palsy: dependence of catch angle on velocity. *Developmental Medicine & Child Neurology*, 52(6):563–569, 2010. doi: https://doi.org/10.1111/j.1469-8749.2009.03602.x.

[16] D.Y. Kim, C. Park, J.S. Chon, S.H. Ohn, T.H. Park, and I.K. Bang. Biomechanical assessment with electromyography of post-stroke ankle plantar flexor spasticity. *Yonsei Medical Journal*, 46(4), 2005. doi: 10.3349/ymj.2005.46.4.546.

[17] R.K. Powers, D.L. Campbell, and W.Z. Rymer. Stretch reflex dynamics in spastic elbow flexor muscles. *Annals of Neurology*, 1989. doi: 10.1002/ana.410250106.

[18] Arjan van der Salm, Peter H. Veltink, Hermie J. Hermens, Maarten J. IJzerman, and Anand V. Nene. Development of a new method for objective assessment of spasticity using full range passive movements. *Archives of Physical Medicine and Rehabilitation*, 86(10):1991–1997, 2005. ISSN 0003-9993. doi: https://doi.org/10.1016/j.apmr.2005.04.023.

[19] D. Burke, J.D. Gillies, and J.W. Lance. Hamstrings stretch reflex in human spasticity. *Journal of Neurology, Neurosurgery & Psychiatry*, 1971. doi: 10.1136/jnnp.34.3.231.

[20] A.F. Thilmann, S.J. Fellow, and E. Garms. The mechanism of spastic muscle hypertonus variation in reflex gain over the time course of spasticity. *Brain*, 114A (1):233–244, 1991. doi: https://doi.org/10.1093/oxfordjournals.brain.a101859.

[21] G. L. Gottlieb and G. C. Agarwal. Response to sudden torques about ankle in man: myotatic reflex. *Journal of Neurophysiology*, 42(1):91–106, 1979. doi: 10.1152/jn.1979.42.1.91.

[22] F. W. J. Cody, Helen C. Ricardson, N. Macdermott, and I. T. Ferguson. Stretch and vibration reflexes of wrist flexor muscles in spasticity. *Brain*, 110(2):

433–450, 04 1987. doi: https://doi.org/10.1093/brain/110.2.433.

[23] Patrick H. McCrea, Janice J. Eng, and Antony J. Hodgson. Linear spring-damper model of the hypertonic elbow: reliability and validity. *Journal of Neuroscience Methods*, 128(1):121–128, 2003. ISSN 0165-0270. doi: https://doi.org/10.1016/S0165-0270(03)00169-9.

[24] A. Berardelli, A.F. Sabra, M. Hallett, W. Berenberg, and S.R. Simon. Stretch reflexes of triceps surae in patients with upper motor neuron syndromes. *Journal of Neurology, Neurosurgery & Psychiatry*, 1983. doi: http://dx.doi.org/10.1136/jnnp.46.1.54.

[25] A. Falisse, L. Bar-on, K. Desloovere, I. Jonkers, and F. De Groote. A spasticity model based on feedback from muscle force explains muscle activity during passive stretches and gait in children with cerebral palsy. *PLOS ONE*, 2018. doi: https://doi.org/10.1371/journal.pone.0208811.

[26] G. Rabita, L. Dupont, A. Thevenon, G. Lensel-Corbeil, C. Pérot, and J. Vanvelcenaher. Differences in kinematic parameters and plantarflexor reflex responses between manual (ashworth) and isokinetic mobilisations in spasticity assessment. *Clinical Neurophysiology*, 2005. doi: 10.1016/j.clinph.2004.07.029.

[27] Lizeth H Sloot, Lynn Bar-On, Marjolein M van der Krogt, Erwin Aertbeliën, Annemieke I Buizer, Kaat Desloovere, and Jaap Harlaar. Motorized versus manual instrumented spasticity assessment in children with cerebral palsy. *Developmental Medicine & Child Neurology*, 59(2):145–151, 2017. doi: https://doi.org/10.1111/dmcn.13194. URL `https://onlinelibrary.wiley.com/doi/abs/10.1111/dmcn.13194`.

[28] R.C. van 't Veld, E.H.F. van Asseldonk, H. van der Kooij, and A.C. Schouten. Disentangling acceleration-, velocity-, and duration-dependency of the short- and medium-latency stretch reflexes in the ankle plantarflexors. *Journal of Neurophysiology*, 2021. doi: https://doi.org/10.1152/jn.00704.2020.

[29] J.M. Finley, Y.Y. Dhaher, and E.J. Perreault. Acceleration dependence and task-specific modulation of short- and medium-latency reflexes in the ankle extensors. *Physiological Reports*, 2013. doi: 10.1002/phy2.51.

[30] Jente Willaert, Kaat Desloovere, Anja Van Campenhout, Lena H. Ting, and Friedl De Groote. Movement history influences pendulum test kinematics in children with spastic cerebral palsy. *Frontiers in Bioengineering and Biotechnology*, 8, 2020. ISSN 2296-4185. doi: 10.3389/fbioe.2020.00920. URL `https://www.frontiersin.org/articles/10.3389/fbioe.2020.00920`.

[31] W.R. Gowers. *A Manual of Diseases of the Nervous System*. London: J. & A. Churchill, 1886. URL `https://wellcomecollection.org/works/wbnkmjub`.

[32] K.P Granata, A.J. Ikeda, and M.F. Abel. Electromechanical delay and reflex response in spastic cerebral palsy. *Archives of Physical Medicine and Rehabilitation*, 2000. doi: 10.1053/apmr.2000.5578.

[33] D.M.Y. Poon and C.W.Y. Hui-Chan. Hyperactive stretch reflexes, co-contraction, and muscle weakness in children with cerebral palsy. *Developmental Medicine & Child Neurology*, 2009. doi: 10.1111/j.1469-8749.2008.03122.x.

[34] M. Willerslev-Olsen, J. Lorentzen, T. Sinkjaer, and J.B. Nielsen. Passive muscle properties are altered in children with cerebral palsy before the age of 3 years and are difficult to distinguish clinically from spasticity. *Developmental Medicine & Child Neurology*, 2013. doi: 10.1111/dmcn.12124.

[35] K. K. Firoozbakhsh, C. F. Kunkel, A. M. Erika Scremin, and M. S. Moneim. Isokinetic dynamometric technique for spasticity assessment. *American Journal of Physical Medicine & Rehabilitation*, 72(6):

379–385, 1993. doi: 10.1097/00002060-199312000-00008.

[36] L. Alibiglou, W.Z. Rymer, R.L. Harvey, and M.M. Mirbagheri. The relation between Ashworth scores and neuromechanical measurements of spasticity following stroke. *Journal of NeuroEngineering and Rehabilitation*, 5, 2008. ISSN 1743-0003. doi: 10.1186/1743-0003-5-18.

[37] M. Mirbagheri, H. Barbeau, M. Ladouceur, and R. Kearney. Intrinsic and reflex stiffness in normal and spastic, spinal cord injured subjects. *Exp Brain Res*, 141:446–459, 2001. doi: https://doi.org/10.1007/s00221-001-0901-z.

[38] Julie G. Pilitsis. Spasticity, 2024. URL `https://bit.ly/3YX0mtC`.

[39] S. Malhotra, E. Cousins, A. Ward, C. Day, P. Jones, C. Roffe, and A. Pandyan. An investigation into the agreement between clinical, biomechanical and neurophysiological measures of spasticity. clinical rehabilitation. *Clinical Rehabilitation*, 22(12):1105–1115, 2008. doi: 10.1177/0269215508095089.

[40] F. Biering-Sørensen, J B Nielsen, and K. Klinge. Spasticity-assessment: a review. *Spinal Cord*, 44(12):708–722, 2006. ISSN 1476-5624. doi: https://doi.org/10.1038/sj.sc.3101928.

[41] A. D. Pandyan, G. R. Johnson, C. I. M. Price, R. H. Curless, M. P. Barnes, and H. Rodgers. A review of the properties and limitations of the ashworth and modified ashworth scales as measures of spasticity. *Clinical Rehabilitation*, 13(5):373–383, 1999. doi: 10.1191/026921599677595404.

[42] G. Tardieu, S. Shentoub, and R. Delarue. A la recherche d'une tecnhnique de mesure de la spasticité. *Rev.Neurol.*, 91:143–144, 1954.

[43] E. Patrick and L. Ada. The tardieu scale differentiates contracture from spasticity whereas the ashworth scale is confounded by it. *Clinical Rehabilitation*, 20:173–182, 2006. doi: 10.1191/0269215506cr922oa.

[44] A. B. Haugh, A. D. Pandyan, and G. R. Johnson. A systematic review of the tardieu scale for the measurement of spasticity. *Disability and Rehabilitation*, 28(15):899–907, 2006. doi: 10.1080/09638280500404305. URL `https://doi.org/10.1080/09638280500404305`.

[45] Jean-Michel Gracies, Kim Burke, Nancy J. Clegg, Richard Browne, Charter Rushing, Darcy Fehlings, Dennis Matthews, Ann Tilton, and Mauricio R. Delgado. Reliability of the tardieu scale for assessing spasticity in children with cerebral palsy. *Archives of Physical Medicine and Rehabilitation*, 91(3):421–428, 2010. ISSN 0003-9993. doi: https://doi.org/10.1016/j.apmr.2009.11.017. URL `https://www.sciencedirect.com/science/article/pii/S0003999309009848`.

[46] Erwin de Vlugt, Jurriaan H. de Groot, Wessel H.J. Wisman, and Carel G.M. Meskers. Clonus is explained from increased reflex gain and enlarged tissue viscoelasticity. *Journal of Biomechanics*, 45(1):148–155, 2012. ISSN 0021-9290. doi: https://doi.org/10.1016/j.jbiomech.2011.09.023. URL `https://www.sciencedirect.com/science/article/pii/S0021929011006269`.

[47] Lizeth H. Sloot, Marjolein M. van der Krogt, Karin L. de Gooijer-van de Groep, Stijn van Eesbeek, Jurriaan de Groot, Annemieke I. Buizer, Carel Meskers, Jules G. Becher, Erwin de Vlugt, and Jaap Harlaar. The validity and reliability of modelled neural and tissue properties of the ankle muscles in children with cerebral palsy. *Gait & Posture*, 42(1):7–15, 2015. ISSN 0966-6362. doi: https://doi.org/10.1016/j.gaitpost.2015.04.006.

[48] K. D. Van de Poll. Estimating ankle muscle parameters. Master's thesis, TU Delft, 2015. URL `http://resolver.tudelft.nl/uuid:aac95ba2-f7f2-4a13-818a-890a42f971e5`.

[49] K.L. de Gooijer-van de Groep. *Identification of neural and non-neural contributors to joint stiffness in up-*

per motor neuron disease. PhD thesis, Revalidatiegeneeskunde, Medicine / Leiden University Medical Center (LUMC), 2019. URL https://scholarlypublications.universiteitleiden.nl/handle/1887/74470.

[50] B.P. van der Ploeg. Separating background activity from noise in emg using a neuromuscular model. Master's thesis, TU Delft, 2015. URL http://resolver.tudelft.nl/uuid:8aeed468-b03d-459c-84fb-84a86570744f.

[51] K.E. Rodriguez Hernandez. *Ankle-Foot-Orthosis "Hermes" Compensates Pathological Ankle Stiffness of Chronic Stroke—A Proof of Concept*. PhD thesis, TU Delft, 2023. URL https://resolver.tudelft.nl/uuid:8bcb339f-3f76-4d19-8644-1bbb7f5023bc.

[52] Aurore Thibaut, Camille Chatelle, Erik Ziegler, Marie-Aurélie Bruno, Steven Laureys, and Olivia Gosseries. Spasticity after stroke: Physiology, assessment and treatment. *Brain Injury*, 27(10):1093–1105, 2013. doi: 10.3109/02699052.2013.804202.

[53] Alessandro Picelli, Gabriella Vallies, Elena Chemello, Paola Castellazzi, Annalisa Brugnera, Marialuisa Gandolfi, Alessio Baricich, Carlo Cisari, Andrea Santamato, Leopold Saltuari, Andreas Waldner, and Nicola Smania. Is spasticity always the same? an observational study comparing the features of spastic equinus foot in patients with chronic stroke and multiple sclerosis. *Journal of the Neurological Sciences*, 380:132–136, 2017. ISSN 0022-510X. doi: https://doi.org/10.1016/j.jns.2017.07.026. URL https://www.sciencedirect.com/science/article/pii/S0022510X17304604.

[54] Aurore Thibaut, Camille Chatelle, Erik Ziegler, Marie-Aurélie Bruno, Steven Laureys, and Olivia Gosseries. Spasticity after stroke: Physiology, assessment and treatment. *Brain Injury*, 27 (10):1093–1105, 2013. doi: 10.3109/02699052.2013.804202. URL https://doi.org/10.3109/02699052.2013.804202.

[55] Sarah F. Eby, Heng Zhao, Pengfei Song, Barbara J. Vareberg, Randall R. Kinnick, James F. Greenleaf, Kai-Nan An, Allen W. Brown, and Shigao Chen. Quantifying spasticity in individual muscles using shear wave elastography. *Radiology Case Reports*, 12(2):348–352, 2017. ISSN 1930-0433. doi: https://doi.org/10.1016/j.radcr.2017.01.004. URL https://www.sciencedirect.com/science/article/pii/S1930043316302837.

[56] Bar-On L, Aertbeliën E, Wambacq H, Severijns D, Lambrecht K, Dan B, Huenaerts C, Bruyninckx H, Janssens L, Van Gestel L, Jaspers E, Molenaers G, and Desloovere K. A clinical measurement to quantify spasticity in children with cerebral palsy by integration of multidimensional signals. *Gait Posture*, 38, 2013. ISSN 1930-0433. doi: 10.1016/j.gaitpost.2012.11.003.

[57] Hermie J Hermens, Bart Freriks, Catherine Disselhorst-Klug, and Günter Rau. Development of recommendations for semg sensors and sensor placement procedures. *Journal of Electromyography and Kinesiology*, 10(5):361–374, 2000. ISSN 1050-6411. doi: https://doi.org/10.1016/S1050-6411(00)00027-4. URL https://www.sciencedirect.com/science/article/pii/S1050641100000274.

[58] Isabel C.N. Sacco, Aline A. Gomes, Mitie E. Otuzi, Denise Pripas, and Andrea N. Onodera. A method for better positioning bipolar electrodes for lower limb emg recordings during dynamic contractions. *Journal of Neuroscience Methods*, 180(1):133–137, 2009. ISSN 0165-0270. doi: https://doi.org/10.1016/j.jneumeth.2009.02.017. URL https://www.sciencedirect.com/science/article/pii/S0165027009001435.

[59] M.A. Cavalcanti Garcia and T.M.M. Vieira. Surface electromyography: Why, when and how to use it. *Revista Andaluza de Medicina del Deporte*, 4(1):17–28, 2011. ISSN 1888-7546. URL https://www.elsevier.es/es-revista-revista-andaluza-medicina-del-deporte-284-

articulo-surface-electromyography-why-when-how-X1888754611201253.

[60] A.A. Kusumojati. Resting period induces time and mechanical history-dependence in muscle thixotropy around the human ankle joint. Master's thesis, TU Delft, 2018. URL https://resolver.tudelft.nl/uuid:582da96a-bbbe-4716-b81b-9039450758a6.

[61] Ricardo Andrade, Lilian Lacourpaille, Sandro Freitas, P McNair, and Antoine Nordez. Effects of hip and head position on ankle range of motion, ankle passive torque, and passive gastrocnemius tension: Hip angle effects on ankle passive mechanical properties. *Scandinavian journal of medicine & science in sports*, 26, 02 2015. doi: 10.1111/sms.12406.

[62] Robert F. Kirsch and Robert E. Kearney. Identification of time-varying stiffness dynamics of the human ankle joint during an imposed movement. *Experimental Brain Research*, 114(1):71–85, March 1997. ISSN 1432-1106. doi: 10.1007/PL00005625. URL https://doi.org/10.1007/PL00005625.

[63] S. P. Magnusson, E. B. Simonsen, P. Dyhre-Poulsen, P. Aagaard, T. Mohr, and M. Kjaer. Viscoelastic stress relaxation during static stretch in human skeletal muscle in the absence of emg activity. *Scandinavian Journal of Medicine & Science in Sports*, 6(6):323–328, 1996. doi: https://doi.org/10.1111/j.1600-0838.1996.tb00101.x. URL https://onlinelibrary.wiley.com/doi/abs/10.1111/j.1600-0838.1996.tb00101.x.

[64] P. J. McNair, E. W. Dombroski, D. J. Hewson, and S. N. Stanley. Stretching at the ankle joint: viscoelastic responses to holds and continuous passive motion. *Medicine and Science in Sports and Exercise*, 33(3):354–358, March 2001. ISSN 0195-9131. doi: 10.1097/00005768-200103000-00003. URL https://doi.org/10.1097/00005768-200103000-00003.

[65] V. Moradi, M.A. Sanjari, and N. Stergiou. Single subject analysis of individual responses to prosthetic modifications based on passive dynamic walking model. *Clinical Biomechanics (Bristol)*, 100:105815, December 2022. ISSN 1879-1271. doi: 10.1016/j.clinbiomech.2022.105815. URL https://doi.org/10.1016/j.clinbiomech.2022.105815.

[66] Gerlienke Voerman, M Gregoric, and Hermie Hermens. Neurophysiological methods for the assessment of spasticity: The hoffman reflex, the tendon reflex, and the stretch reflex. *Disability and rehabilitation*, 27:33–68, 01 2005. doi: 10.1080/09638280400014600.

[67] J. Harlaar, J.G. Becher, C.J. Snijders, and G.J. Lankhorst. Passive stiffness characteristics of ankle plantar flexors in hemiplegia. *Clinical Biomechanics*, 15(4):261–270, 2000. ISSN 0268-0033. doi: https://doi.org/10.1016/S0268-0033(99)00069-8. URL https://www.sciencedirect.com/science/article/pii/S0268003399000698.

[68] Karl F. Orishimo, Gideon Burstein, Michael J. Mullaney, Ian J. Kremenic, Marcus Nesse, Malachy P. McHugh, and Steven J. Lee. Effect of knee flexion angle on achilles tendon force and ankle joint plantarflexion moment during passive dorsiflexion. *The Journal of Foot and Ankle Surgery*, 47(1):34–39, 2008. ISSN 1067-2516. doi: https://doi.org/10.1053/j.jfas.2007.10.008. URL https://www.sciencedirect.com/science/article/pii/S1067251607003870.

A Inertia

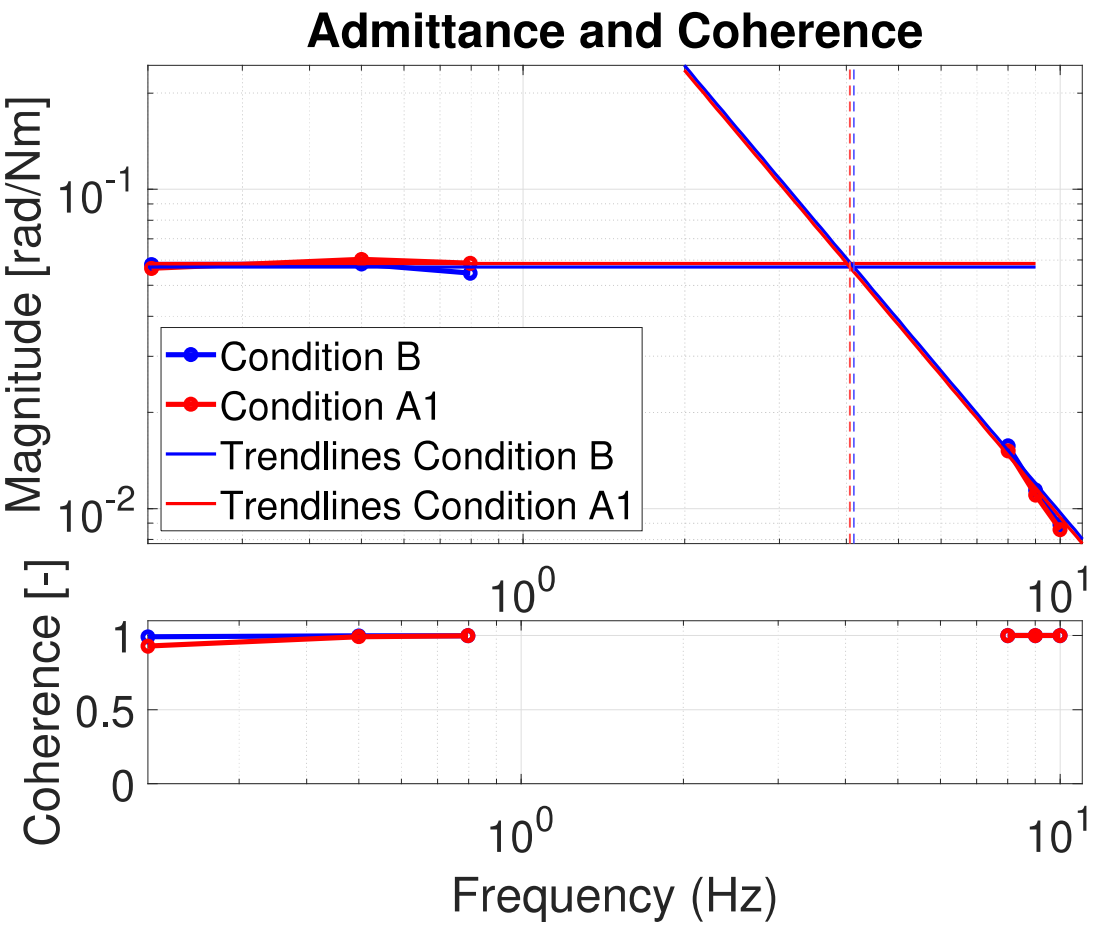

Figure 11: Admittance and coherence of the transfer function of the multi-sine used for the inertia test under conditions baseline (B) (blue), and alignment 1 (A1) (red). Input: Position. Output Torque. Top panel: Magnitude of the admittance. Trendlines are based on lower-frequency and higher-frequency data points. Intersections indicate the estimated eigenfrequency of the ankle. Bottom panel: Coherence between the position and torque signals at each frequency.

B Torques Participant P1

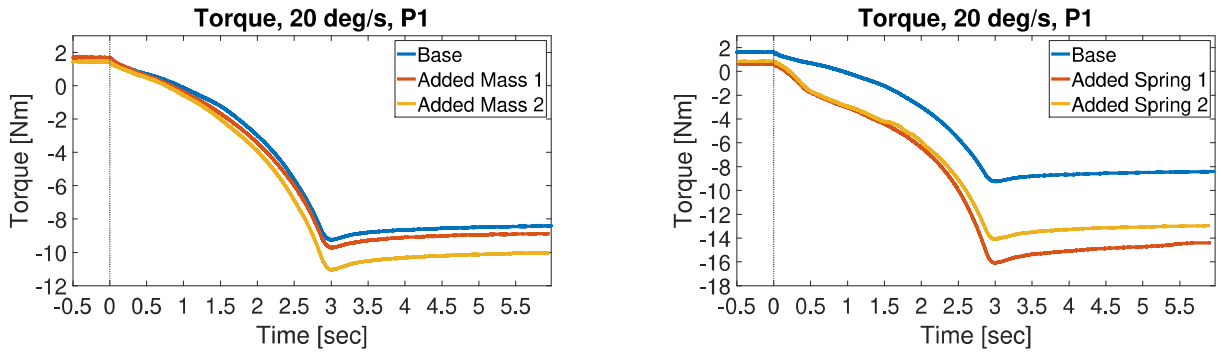

Figure 12: Means of torque profiles. Ramp-and-hold from plantarflexed to dorsiflexed position starts at 0 sec. Left panel: conditions 'Base' (blue), 'Added Mass 1' (orange), and 'Added Mass 2' (yellow) at 20 deg/s of participant P1. Middle panel: Conditions 'Base' (blue), 'Added Spring 1' (orange), and 'Added Spring 2' (yellow) at 20 deg/s of participant P1.

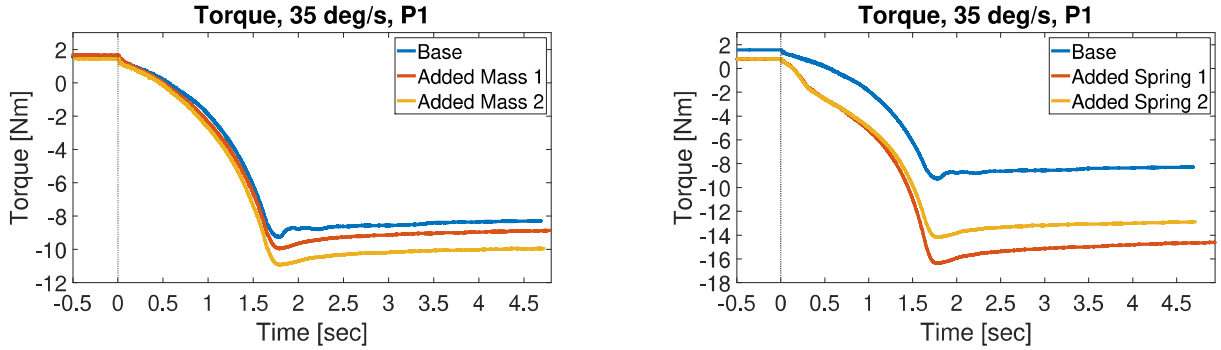

Figure 13: Means of torque profiles. Ramp-and-hold from plantarflexed to dorsiflexed position starts at 0 sec. Left panel: conditions 'Base' (blue), 'Added Mass 1' (orange), and 'Added Mass 2' (yellow) at 35 deg/s of participant P1. Middle panel: Conditions 'Base' (blue), 'Added Spring 1' (orange), and 'Added Spring 2' (yellow) at 35 deg/s of participant P1.

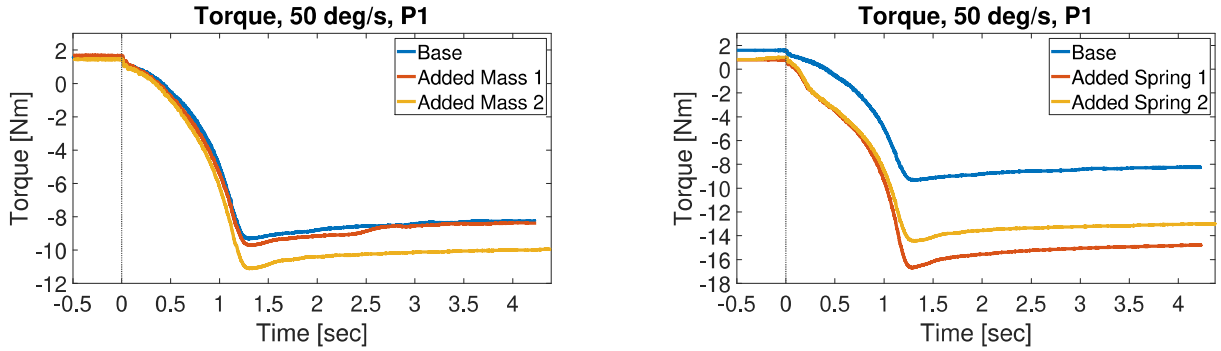

Figure 14: Means of torque profiles. Ramp-and-hold from plantarflexed to dorsiflexed position starts at 0 sec. Left panel: conditions 'Base' (blue), 'Added Mass 1' (orange), and 'Added Mass 2' (yellow) at 50 deg/s of participant P1. Middle panel: Conditions 'Base' (blue), 'Added Spring 1' (orange), and 'Added Spring 2' (yellow) at 50 deg/s of participant P1.

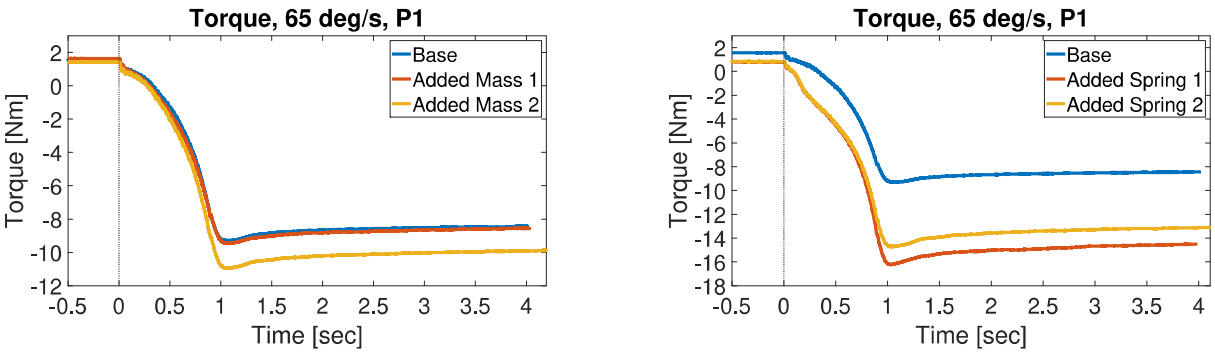

Figure 15: Means of torque profiles. Ramp-and-hold from plantarflexed to dorsiflexed position starts at 0 sec. Left panel: conditions 'Base' (blue), 'Added Mass 1' (orange), and 'Added Mass 2' (yellow) at 65 deg/s of participant P1. Middle panel: Conditions 'Base' (blue), 'Added Spring 1' (orange), and 'Added Spring 2' (yellow) at 65 deg/s of participant P1.

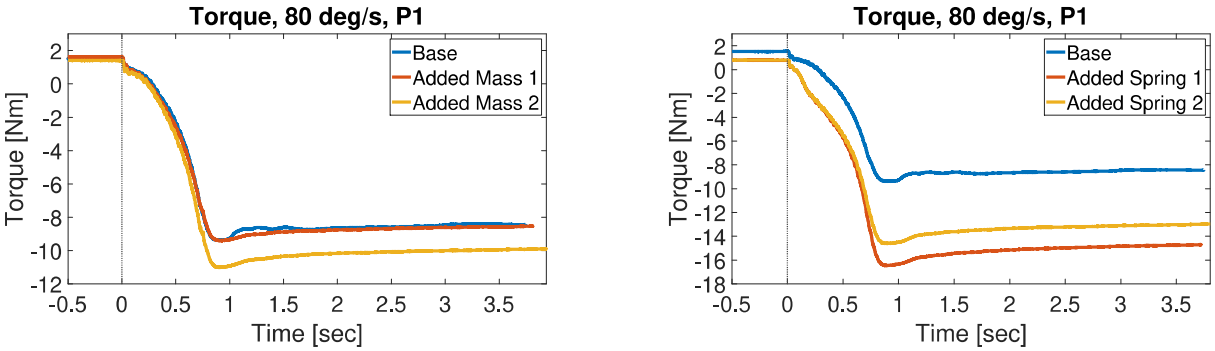

Figure 16: Means of torque profiles. Ramp-and-hold from plantarflexed to dorsiflexed position starts at 0 sec. Left panel: conditions 'Base' (blue), 'Added Mass 1' (orange), and 'Added Mass 2' (yellow) at 80 deg/s of participant P1. Middle panel: Conditions 'Base' (blue), 'Added Spring 1' (orange), and 'Added Spring 2' (yellow) at 80 deg/s of participant P1.

C Torques Participant P2

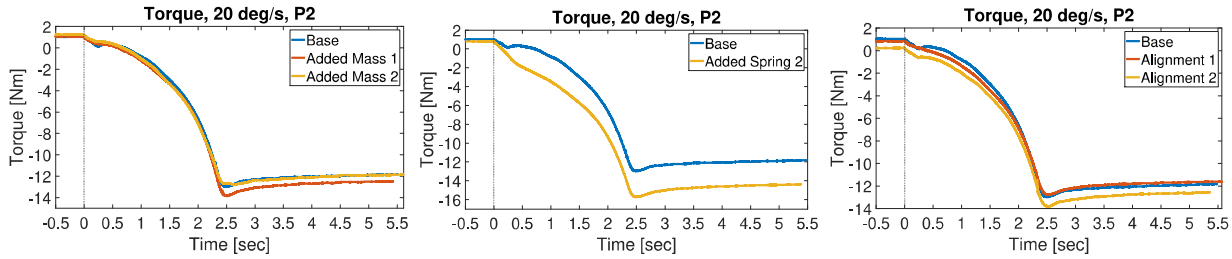

Figure 17: Means of torque profiles. Ramp-and-hold from plantarflexed to dorsiflexed position starts at 0 sec. Left panel: conditions 'Base' (blue), 'Added Mass 1' (orange), and 'Added Mass 2' (yellow) at 20 deg/s of participant P2. Middle panel: Conditions 'Base' (blue), 'Added Spring 1' (orange), and 'Added Spring 2' (yellow) at 20 deg/s of participant P2. Left panel: Conditions 'Base' (blue), 'Alignment 1' (orange), and 'Alignment 2' (yellow) at 20 deg/s of participant P2.

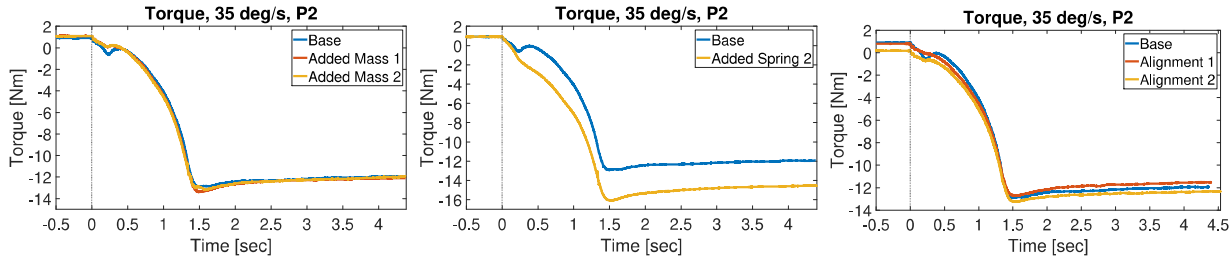

Figure 18: Means of torque profiles. Ramp-and-hold from plantarflexed to dorsiflexed position starts at 0 sec. Left panel: conditions 'Base' (blue), 'Added Mass 1' (orange), and 'Added Mass 2' (yellow) at 35 deg/s of participant P2. Middle panel: Conditions 'Base' (blue), 'Added Spring 1' (orange), and 'Added Spring 2' (yellow) at 35 deg/s of participant P2. Left panel: Conditions 'Base' (blue), 'Alignment 1' (orange), and 'Alignment 2' (yellow) at 35 deg/s of participant P2.

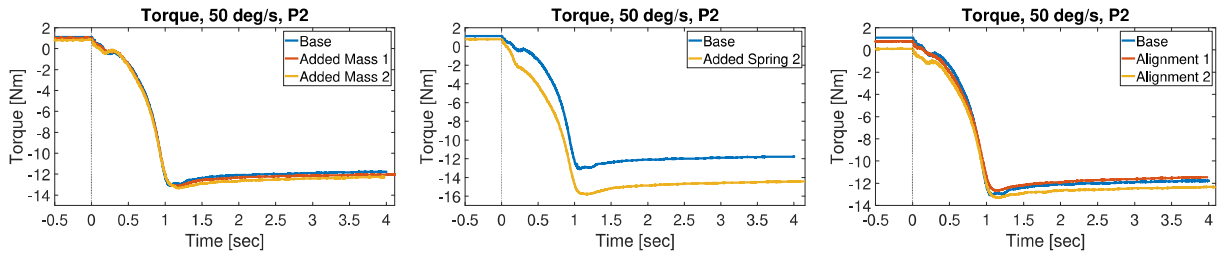

Figure 19: Means of torque profiles. Ramp-and-hold from plantarflexed to dorsiflexed position starts at 0 sec. Left panel: conditions 'Base' (blue), 'Added Mass 1' (orange), and 'Added Mass 2' (yellow) at 50 deg/s of participant P2. Middle panel: Conditions 'Base' (blue), 'Added Spring 1' (orange), and 'Added Spring 2' (yellow) at 50 deg/s of participant P2. Left panel: Conditions 'Base' (blue), 'Alignment 1' (orange), and 'Alignment 2' (yellow) at 50 deg/s of participant P2.

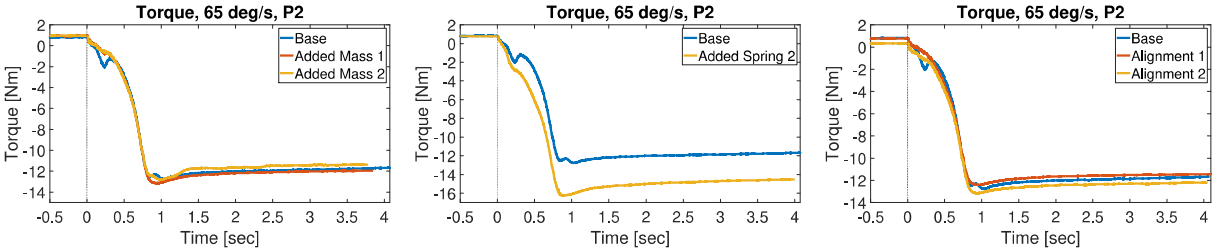

Figure 20: Means of torque profiles. Ramp-and-hold from plantarflexed to dorsiflexed position starts at 0 sec. Left panel: conditions 'Base' (blue), 'Added Mass 1' (orange), and 'Added Mass 2' (yellow) at 65 deg/s of participant P2. Middle panel: Conditions 'Base' (blue), 'Added Spring 1' (orange), and 'Added Spring 2' (yellow) at 65 deg/s of participant P2. Left panel: Conditions 'Base' (blue), 'Alignment 1' (orange), and 'Alignment 2' (yellow) at 65 deg/s of participant P2.

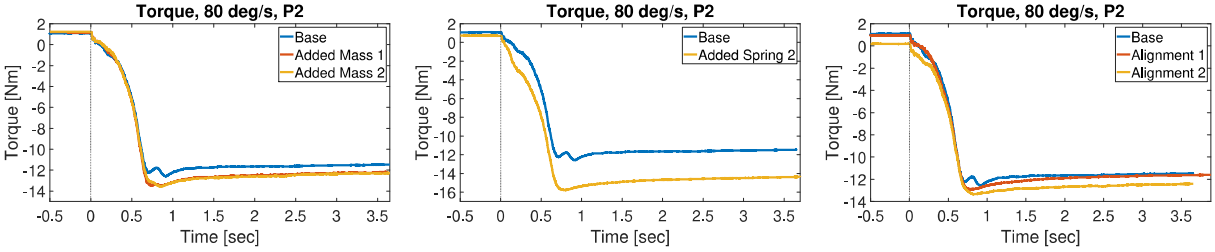

Figure 21: Means of torque profiles. Ramp-and-hold from plantarflexed to dorsiflexed position starts at 0 sec. Left panel: conditions 'Base' (blue), 'Added Mass 1' (orange), and 'Added Mass 2' (yellow) at 80 deg/s of participant P2. Middle panel: Conditions 'Base' (blue), 'Added Spring 1' (orange), and 'Added Spring 2' (yellow) at 80 deg/s of participant P2. Left panel: Conditions 'Base' (blue), 'Alignment 1' (orange), and 'Alignment 2' (yellow) at 80 deg/s of participant P2.

D Modeled Sensitivity Analysis

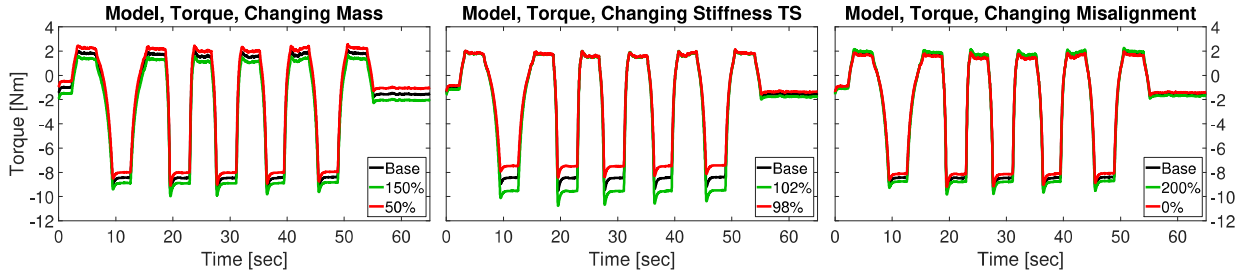

Figure 22: Estimated torque outputs of the sensitivity analysis of the model with base data of participant P1. Left panel: The mass parameter is tested at base or 100% (black), 150% (green), and 50% (red). Middle panel: The triceps surae stiffness parameter is tested at base or 100% (black), 102% (green), and 98% (red). Left panel: The misalignment parameter is tested at base or 100% (black), 200% (green), and 0% (red).

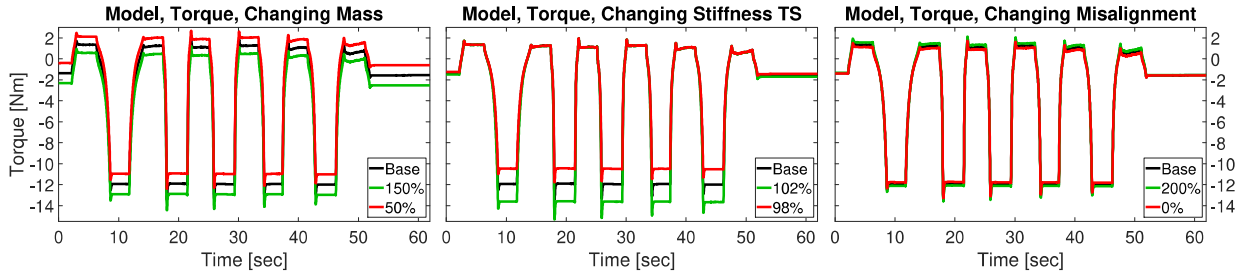

Figure 23: Estimated torque outputs of the limited sensitivity analysis of the model with base data of participant P2. Left panel: The mass parameter is tested at base or 100% (black), 150% (green), and 50% (red). Middle panel: The triceps surae stiffness parameter is tested at base or 100% (black), 102% (green), and 98% (red). Left panel: The misalignment parameter is tested at base or 100% (black), 200% (green), and 0% (red).

E All Optimized Parameters

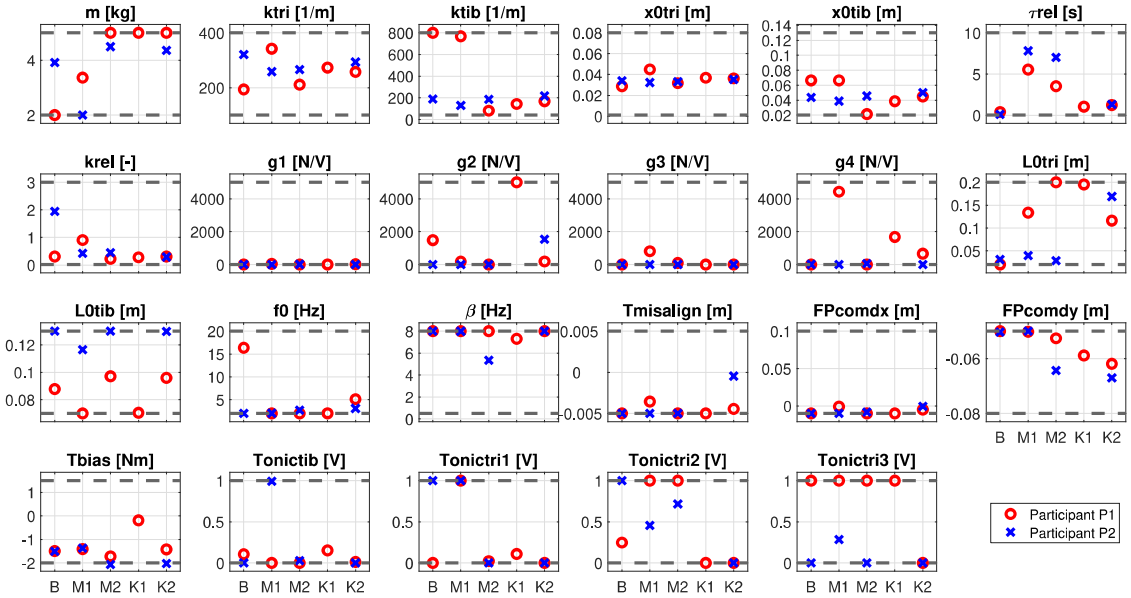

Figure 24: All optimized parameter values for conditions baseline (B), added mass 1 (M1), added mass 2 (M2), added spring 1 (K1), and added spring 2 (K2) for participants P1 and P2. Overview of model parameters and abbreviations: m - mass; ktri - stiffness of triceps surae (TS); ktib - stiffness of tibialis anterior (TA); x0tri - slack length of triceps surae; x0tib - slack length of TA; τrel - relaxation time constant; krel - relaxation factor; g1 - EMG weight factor for TA; g2 - EMG weight factor for gastrocnemius lateralis (GL); g3 - EMG weight factor for soleus (SOL); g4 - EMG weight factor for gastrocnemius medialis (GM); l0tri - optimal muscle length of TS; l0tib - optimal muscle length of TA; f0 - cut-off frequency of activation filter; β - relative damping coefficient of activation filter; Tmisalign - misalignment of ankle joint; FPcomdx and FPcomdy - x and y positions of footplate center of mass in local coordinates; Tbias - bias torque; Tonictib - noise of TA; Tonictri1, Tonictri2, Tonictri3 - noise of GL, SOL, and GM, respectively.